การตรวจสอบโครงสร้างและการสะสมไฮโดรเจนของแผ่นซิงก์ออกไซด์
ระดับนาโนเมตรชนิดหลายชั้น

นางสาวชลิตา เมฆมุกดา

วิทยานิพนธ์นี้เป็นส่วนหนึ่งของการศึกษาตามหลักสูตรปริญญาวิทยาศาสตรมหาบัณฑิต
สาขาวิชาเคมี ภาควิชาเคมี
คณะวิทยาศาสตร์ จุฬาลงกรณ์มหาวิทยาลัย
ปีการศึกษา 2555
ลิขสิทธิ์ของจุฬาลงกรณ์มหาวิทยาลัย

STRUCTURAL INVESTIGATION AND HYDROGEN STORAGE OF
MULTILAYER ZnO NANOSHEETS

Miss Chalita Mekmukda

A Thesis Submitted in Partial Fulfillment of the Requirements
for the Degree of Master of Science Program in Chemistry
Department of Chemistry
Faculty of Science
Chulalongkorn University
Academic Year 2012

Thesis Title   STRUCTURAL INVESTIGATION AND HYDROGEN
                      STORAGE OF MULTILAYER ZnO NANOSHEETS

By   Miss Chalita Mekmukda

Field of study   Chemistry

Thesis Advisor   Associate Professor Vithaya Ruangpornvisuti, Dr.rer.nat.

        Accepted by the Faculty of Science, Chulalongkorn University in Partial Fulfillment of the Requirements for the Master's Degree

        …………………………………….Dean of the Faculty of Science
        (Professor Supot Hannongbua, Dr.rer.nat.)

THESIS COMMITTEE

        …………………………..............Chairman
        (Assistant Professor Warinthorn Chavasiri, Ph.D.)

        …………………………..............Thesis Advisor
        (Associate Professor Vithaya Ruangpornvisuti, Dr.rer.nat.)

        …………………………..............Examiner
        (Kanet Wongravee, Ph.D.)

        …………………………..............External Examiner
        (Banchob Wanno, Ph.D.)

ชลิตา เมฆมุกดา : การตรวจสอบโครงสร้างและการสะสมไฮโดรเจนของแผ่นซิงก์ออกไซด์ระดับนาโนเมตร . (STRUCTURAL INVESTIGATION AND HYDROGEN STORAGE OF MULTIGATION ZnO NANOSHEETS) อ. ที่ปรึกษาวิทยานิพนธ์หลัก: รศ. ดร.วิทยา เรืองพรวิสุทธิ์, 64 หน้า.

ศึกษาโครงสร้างที่เหมาะสมของ แผ่นนาโน ซิงก์ออกไซด์ ชนิดคล้ายกราฟีน ชั้นเดียว (ZnGLNS) ได้แก่ ชนิดคล้าย ไพรีน (PRL–ZnONS), ชนิดคล้าย โคโรนีน (CNL–ZnONS) และชนิดคล้ายเซอคัมโคโรนีน (CCL–ZnONS) และชนิดหลายชั้น ได้แก่ (PRL–ZnONS)$_n$, (CNL–ZnONS)$_n$ และ (CCL–ZnONS)$_n$ (n = 2 ถึง 4) และโครงสร้างที่ไม่มีไฮโดรเจนที่ขอบของโมเลกุลเหล่านี้หาได้ โดยการคำนวณด้วย วิธี B3LYP/LanL2DZ พลังงานไฮโดรจีเนชันของสารประกอบ ZnOGLNSs ต่างๆ และพลังงานที่เกี่ยวข้อง ได้รับการรายงานการศึกษาการเกิดการเพิ่มชั้นของแผ่นนาโนซิงก์ออกไซด์ชนิดคล้ายกราฟีนชั้นเดียวแบบไม่มีและมีไฮ   โครเจนอะตอมที่ขอบ และการคำนวณพลังงานการรวมตัวดังกล่าว และได้ ศึกษาโครงสร้างการดูดซับของแก๊สแอมโมเนียและน้ำ บนแผ่นนาโนซิงก์ออกไซด์ชนิดคล้ายโคโรนีน พลังงานการดูดซับของแก๊สแอมโมเนียบน แผ่นนาโนซิงก์ออกไซด์ชนิดคล้าย โคโรนีนมีค่าอยู่ระหว่าง –28.25 ถึง –21.52 กิโลแคลอรีต่อโมล และพลังงานการดูดซับของน้ำบน แผ่นนาโนซิงก์ออกไซด์ชนิดคล้าย โคโรนีน มีค่าอยู่ระหว่าง –40.18 ถึง –12.03 กิโลแคลอรีต่อโมล และได้คำนวณค่าแถบพลังงาน และค่าดัชนีเคมีกัลป์

ภาควิชา___เคมี___ลายมือชื่อนิสิต...
สาขาวิชา___เคมี___ลายมือชื่อ อ.ที่ปรึกษาวิทยานิพนธ์หลัก....................................
ปีการศึกษา__2555_____

#5471945523: MAJOR CHEMISTRY

KEYWORDS: HYDROGEN STORAGE; MULTILAYERIZATION, ZnO-NANOSHEETS; ZnOGLNS; DFT; ADSORPTION ENERGY; AMMONIA; WATER

CHALITA MEKMUKDA: STRUCTURAL INVESTIGATION AND HYDROGEN STORAGE OF MULTILAYER ZnO NANOSHEETS. ADVISOR: ASSOC. PROF. VITHAYA RUANGPORNVISUTI, Dr.rer.nat. , 64 pp.

The structures of ZnO graphene–like nanosheets (ZnOGLNSs) i.e. pyrene–like (PRL–ZnONS), coronene–like (CNL–ZnONS), circumcoronene–like (CCL–ZnONS), their multi–layers $(PRL–ZnONS)_n$, $(CNL–ZnONS)_n$, $(CCL–ZnONS)_n$, (n= 2 to 4) and their non–terminated structures were obtained using B3LYP/LanL2DZ calculations. Hydrogenation energies of all studied ZnOGLNSs and their related energies are reported. Multilayerization of single–layer of non– and hydrogen–terminated PRL–ZnONS, CNL–ZnONS and CCL–ZnONS to afford their double–, triple– and quadruple–layers were studied and their binding energies were obtained. Adsorption configurations of NH_3 and H_2O on single–, double–, triple– and quadruple–layer CNL–ZnOGLNSs and their adsorption energies were obtained. Adsorption energies of CNL–ZnOGLNS and its multi–layers species are within the range of –28.25 to –21.52 kcal/mol for NH_3 and –40.18 to –12.03 kcal/mol for H_2O, respectively. Energy gaps, chemical indices of CNL–ZnOGLNS and its multi–layers species are reported.

Department: Chemistry   Student's Signature ⋯⋯⋯⋯⋯⋯⋯⋯⋯

Field of Study: Chemistry   Advisor's Signature ⋯⋯⋯⋯⋯⋯⋯⋯⋯

Academic Year: 2012

ACKNOWLEDGEMENTS

This study was carried out at the Department of Chemistry, Faculty of Science, Chulalongkorn University.

I would like to really thank to my advisor Associate Professor Vithaya Ruangpomvisuti for his patient guidance, enthusiastic encourangement, useful critiques of this research work for over the years. His willingness to spend his time so generously has been very much appreciated.

My grateful thanks are also extended to Assist. Prof. Dr. Warinthorn Chavasiri, Dr. Kanet Wongravee and Dr. Banchob Wanno for spending their time for recommendation of my thesis.

I would also like to thank the members of my laboratory for their helps.

Finailly, I would like to thank my parents for giving birth to me at the first place, supporting me spiritually throughout my life and standing beside me. They always love me and I am very proud to be a part of my family.

CONTENTS

Page

LIST OF TABLES

LIST OF FIGURES

Figure   **Page**

LIST OF ABBREVIATIONS

Å	Angstrom
B3LYP	Beck 3 Lee–Yang–Parr
BS	Bond strength
CCL	Circumcoronene–like
CNL	Coronene–like
$c_{\mu i}$	Coefficients
DFT	Density functional theory
E	Energy
ECP	Effective core potentials
$\hat{H}$	Hamiltonian operator
HF	Hartree–Fock
LanL2DZ	Los Alamos National Laboratory 2 double Zeta
NBO	Natural bond orbital
N_o	Avogadro number
N_{TP}	Termination-proton numbers
PRL	Pyrene–like
ZnO	Zinc oxide
ZnONSs	Zinc oxide nanosheets
ψ	Wave function
ϕ	Basis functions
ρ	Electron density
IP	Ionization potential
EA	Electron affinity
μ	Electronic chemical potential
χ	Mulliken electronegativity
ω	Electrophilicity
S	Global softness
η	Chemical hardness

CHAPTER I

INTRODUCTION

1.1 Background and Literature reviews

The structures and optoelectronic properties of unsaturated ZnO and ZnS nanoclusters were studied using density functional theory (DFT) and their optical gap were computed using TDDFT (Time–Dependent DFT) [1] and they have been investigated by means of Car–Parrinello molecular dynamics [2]. The growth pattern and electronic properties of $Zn_{12}O_{12}$–assembled material were studied using DFT and its phases were found to be semiconductor with large gap value [3]. The impact of hydrogen and water molecules on zinc oxide clusters $(ZnO)n =3–6$ was investigated using DFT calculation [4]. The structural, electronic, magnetic properties and relative stabilities of fully and partially hydrogenated ZnO nanosheets were investigated by DFT method and it was found that full hydrogenation is more favorable energetically for thinner ZnO nanosheets, whereas semihydrogenation at O sites is favored for thicker ones [5]. There are three types of ZnO crystal structure such as rocksalt, hexagonal and wurtzite structure as shown in Figure 1.1 [6].

(a) rock salt   (b) zinc blende   (c) wurtzite
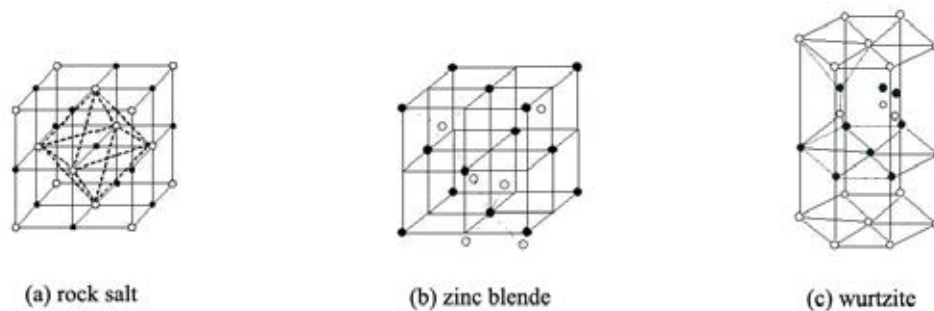
Figure 1.1 Structures of ZnO clusters (a) rocksalt, (b) zinc blende and (c) wurtzite. Black balls denote Zn and O atoms, respectively.

DFT structures of $(ZnO)_n$ (n = 1–12) clusters as ring and three–dimensional structures were found but their ring structure of n > 10 does not exist [7]. The structural and electronic properties of $(ZnO)_n$ n = 2–18) clusters were studied using gradient–corrected DFT method [8]. The energetics, stable configurations and electronic structures of the $(ZnO)_n$ clusters for n ranging from 9 to 64 were studied by using first–principles calculations [9]. The atomic structures of small zinc oxide clusters $(ZnO)_n$ n ≤ 6 using ultrasoft pseudopotential method and the generalized gradient approximation for the exchange–correlation energy were studied [10]. The structures and electronic properties of ZnO single crystals obtained by means of both conventional hydrothermal and microwave–hydrothermal synthesis methods were studied [11]. The structures and electronic properties of zinc oxide (ZnO) one–dimensional (1D) nanostructures, including nanowires with hexagonal or triangular cross sections, faceted nanotubes, and conventional single–walled nanotubes, were investigated using DFT method [12]. ZnO nanosheets were synthesized by a sonochemical method and characterized by powder X–ray diffraction (XRD) and scanning electron microscopy (SEM) [13]. Hydrogen adsorptions on large $(ZnO)_{60}$ cluster models using AM1 semi–empirical method. [14] and on ZnO ($10 1 \overline{0}$) surface has been investigated by means of ab initio embedded cluster method [15].

As hydrogen using for fuel cell is the most promising alternative to fossil fuel, numerous works of finding materials for hydrogen storage have been widely investigated [16–42]. Since hydrogen–terminated ZnO graphene–like nanosheets (ZnOGLNSs) as novel materials were proposed as high ability for small gases adsorptions [43–45], their ability for hydrogen molecules storage in their molecules have interested many scientists including us to study their adsorption and release hydrogen for using in fuel cell.

The faces of several ZnO crystals have been studied by several theoretical and experimental methods and their strong adsorptions of H_2O [46–48] and NH_3 [49] were found to be high. Nevertheless, H_2O and NH_3 adsorptions [50] on hydrogen–terminated ZnO graphene–like nanosheets (ZnOGLNSs) materials were early studied.

1.2 Objective

From literature reviews, it is seen that there was still no research about hydrogen storage and adsorption on multiple Zinc oxide graphene–like nanosheets (ZnOGLNS). In this study, stabilities of three sizes of Zinc oxide graphene like nanosheets such as pyrene–like (PRL–ZnONS, $Zn_8O_8H_{10}$), coronene–like (CNL–ZnONS, $Zn_{12}O_{12}H_{12}$), circumcoronene–like (CCL–ZnONS, $Zn_{27}O_{27}H_{18}$), their double–, triple– and quadruple–layer forms compared with their dehydrogenated forms and have been studied. Hydrogen molecular up–take for all studied compounds have been determined. The coronene–like ZnO graphene–like nanosheet (CNL–ZnOGLNS) and its double–, triple– and quadruple–layer species have been studied of adsorption. Their electronic properties have also been investigated. Adsorption abilities of H_2O and NH_3 on these nanosheets have been expected to be useful information for sensor application of these materials.

CHAPTER II

THEORETICAL BACKGROUND

Quantum chemistry is a basis of physical chemistry which consists of semi–empirical, Hartree–Fock (HF) and DFT methods. Both are mainly functional methods for using behavioral anticipation and description. Especially, during chemical reaction, quantum chemical investigated conduct of individual atoms and molecules in ground state, excited state and transition state.

2.1 The HF method

Ab initio methods are the integral associated with Schrödinger equation and unused the empirical parameters [51].

$$\hat{H}\Psi = E\Psi \qquad (2.1)$$

E is the total energy of the system

Ψ is the *n*–electron wave function

$\hat{H}$ is Hamiltonian operator

The HF method [52–55] is approximated method for using described and determinate on ground state wave function and ground state energy of a quantum many body system [53].

The Hamiltonian $\hat{H}$ function was described that assigned the formula as specifying the kinetic and potential energies for each of the particles:

$$\hat{H} = -\frac{\overline{h}^2}{2m_e}\sum_{i}^{electrons}\nabla_i^2 - \frac{\overline{h}^2}{2}\sum_{A}^{nuclei}\frac{1}{M_A}\nabla_A^2 - \frac{e^2}{4\pi\varepsilon_0}\sum_{i}^{electrons}\sum_{A}^{nuclei}\frac{Z_A}{r_{iA}}$$
$$+ \frac{e^2}{4\pi\varepsilon_0}\sum_{i>}^{electrons}\sum_{j}^{electrons}\frac{1}{r_{ij}} + \frac{e^2}{4\pi\varepsilon_0}\sum_{A>}^{nuclei}\sum_{B}^{nuclei}\frac{Z_A Z_B}{R_{AB}} \qquad (2.2)$$

The $\hat{H}$ operator in equation (2.2) represent to ground state energy.

2.2 DFT method

The basis of DFT [56–57] is determination of ground state electronic energy by electron density (ρ). DFT is depended not upon the wavefunction, although it is more related on the electron probability density function or electron density function, called simply the electron density or charge density. The HF model is commonly and understanding as DFT. The density function is assumed that depended on availability of right solution for an idealized many–electron problem, especially the uniformed density of electron gas. From the section of this, it associates with only to the exchange, moreover it is correlated contributions is extracted and in addition this is exactly included into the SCF formalism that similar with HF formalism.

The HF energy is presented as a combination following below. The all of them is components of the electron-electron interaction energy:

$$E^{HF} = E_T + E_V + E_J + E_K \tag{2.3}$$

Where E_T is kinetic energy

E_V is the electron-nuclear potential energy

E_J is coulomb's energy

E_K is exchange's energy

From the three energy part in first of these terms take hold from to density functional models of the HF exchange energy. In equation (2.3) is substituted by so–called exchange/correlation energy, E_{XC} which the form follows from the pattern of the idealized electron gas problem:

$$E^{DFT} = E_T + E_V + E_J + E_{XC} \tag{2.4}$$

Although, it is excepted in E_T, all operation in this formula based on the total electron density, $\rho(r)$:

$$\rho(r) = 2 \sum_{i}^{orbitals} \left| \psi_i(r) \right|^2 \tag{2.5}$$

The ψ_i are orbitals that it is exactly like to molecular orbitals in HF theory.

2.2.1 Hybrid methods

Hybrid functional increase the DFT exchange–correlation energy with a term calculated from Hartree–Fock theory. The Kohn–Sham orbitals are quit similar to the HF orbitals give an expression for the HF exchange energy [57–58].

$$E_x^{HF} = -\sum_{i=1}^{n} \sum_{j=1}^{n} \left\langle \psi_i^{KS}(1)\psi_i^{KS}(2) \left| \frac{1}{r_{ij}} \right| \psi_i^{KS}(2)\psi_j^{KS}(1) \right\rangle \tag{2.6}$$

2.3 Gaussian basis sets

The basis sets [57] are a set of mathematical functions, which are expanded by means of linear combination of atomic orbitals (LCAO). These function was not cost effective, and early numerical calculations were carried out using Slater–type orbitals (STOs),

$$\phi(r,\theta,\phi) = \frac{(2\zeta / a_0)^{n+1/2}}{[(2n)!]^{1/2}} r^{n-1} e^{-\zeta r/a_0} Y_l^m(\theta,\phi) \tag{2.7}$$

Further work showed that the cost of calculations can be further reduced if the AOs are expanded in terms of Gaussian functions, which have the form

$$g_{ijk}(r) = N x^i y^j z^k e^{-\alpha r^2} \tag{2.8}$$

2.3.1 Minimal basis sets

Minimal basis sets were shown the lowest sum of basis function necessary for every atom, which used permanent size atomic type orbitals. The minimal basis sets base on STO–3G [56].

$$\varphi(2s) \ = d_{1s}e^{-\alpha_{1s}r} + d_{2s}e^{-\alpha_{2s}r} + d_{3s}e^{-\alpha_{3s}r}$$
$$\phi(2p_x) = d_{1p_x}e^{-\alpha_{1p}r} + d_{2p_x}e^{-\alpha_{2p}r} + d_{3p_x}e^{-\alpha_{3p}r}$$
$$\phi(2p_y) = d_{1p_y}e^{-\alpha_{1p}r} + d_{2p_y}e^{-\alpha_{2p}r} + d_{3p_y}e^{-\alpha_{3p}r}$$
$$\phi(2p_z) = d_{1p_z}e^{-\alpha_{1p}r} + d_{2p_z}e^{-\alpha_{2p}r} + d_{3p_z}e^{-\alpha_{3p}r}$$

2.3.2 Effective core potentials

For the core potential study, effective core potentials (ECP) have been the highly performance in the molecular orbital calculations that use suitable with transition metals. From many researches, the LanL2DZ basis set [53] was selected for investigated in geometry optimization. It contains effective core potential representations of electrons near the nuclei for post–third–row atoms.

2.4 The chemical indices

DFT is easy visualization and big advantage. The electron number N has a central place. After all, much of chemistry is about the transfer of electrons from one place to another [59].

2.4.1 Electronic chemical potential

The chemical potential of the DFT [59] variational the principle of equation (2.9) is a very small one-electron energy that is smaller than the totalelectronic energy E which gets into the variational principle of traditional quantum chemistry.

$$\delta\{E[\eta(r)] - \mu[N[\eta(r)]]\} = 0 \tag{2.9}$$

Where μ is a electronic chemical potential, η is a chemical hardness and N is a electron molecular system.

It has to solve this equation for every μ and then choosing the μ value that takes the correct number of electrons for the system of interest. According to the Lagrange multipliers, μ measures how sensitive the extremum E is to a change in N.

$$\mu = \left(\frac{\partial E}{\partial N}\right)_{V(\bar{r})} \tag{2.10}$$

This equation (2.8) shows how to approximate of μ, ionization potential IP and electron affinity EA in the differential way.

$$\mu \approx -\frac{1}{2}(IP + EA) \tag{2.11}$$

2.4.2 Mulliken electronegativity

This equation is shown about the mulliken electronegativity (χ) [59–60] that is a negative of chemical potential in DFT.

$$\chi = -\mu \tag{2.12}$$

2.4.3 Chemical hardness-softness

The hardness [60–69] can be thought of as a resistance to charge transfer. The softness measures relieve of transfer; softness is associated with high polarizability.

E versus N plots are not straight lines but are generally convex upward. Their curvatures define another property of substantial importance, the hardness.

$$\eta = \left(\frac{\partial^2 E}{\partial N^2} \right)_{v(\bar{r})} \tag{2.13}$$

The finite-difference approximation is shown in equation [67]

$$\eta \approx \frac{1}{2}(IP - EA) \tag{2.14}$$

To merge the site reactivity index $f(r)$ with the global softness measure (S), the local softness is an important quantity.

$$S \approx \frac{1}{(IP - EA)} \quad \text{or} \quad S = \frac{1}{2\eta} \tag{2.15}$$

2.4.4 Electrophilicity

The electrophilicity (ω) index [69–73] is a reliable property of a chemical system and may be used as quantum chemical descriptor, the operational definition of electrophilicity index may be written as:

$$\omega = \frac{\mu^2}{2\eta} \tag{2.16}$$

CHAPTER III

DETAILS OF THE CALCULATIONS

3.1 Computational method

The structure optimizatios are pyrene–like (PRL–ZnONS, $Zn_8O_8H_{10}$), coronene–like (CNL–ZnONS, $Zn_{12}O_{12}H_{12}$), circumcoronene–like (CCL–ZnONS, $Zn_{27}O_{27}H_{18}$), their double–, triple– and quadruple–layer forms were carried out using density functional theory method. The hybrid density functional B3LYP, the Becke three–parameter hybrid functional [51] combined with the Lee–Yang–Parr correlation functional [52], using the Los Alamos LanL2DZ split–valence basis set [53–55] have been employed in calculations. All calculations were performed with the Gaussian 03 program [55–57].

The B3LYP/LanL2DZ–optimized structures of non– and hydrogen–terminated forms of the PRL–ZnONS, CNL–ZnONS and CCL–ZnONS were obtained as shown in Figure 3.1. It shows the molecular symmetries for non– and hydrogen–terminated structures of the PRL–ZnONS, CNL–ZnONS and CCL–ZnONS.

3.2 Definitions of reaction terms

3.2.1 Binding of multi–layer ZnOGLNSs

Binding of single–layer ZnOGLNS to be double–, triple– and quadruple–layer ZnOGLNSs is defined as following equations.

For stepwise processes of PRL–ZnONS as representative compound:

$$\text{PRL–ZnONS} \quad + \text{ PRL–ZnONS} \quad \rightarrow \text{ (PRL–ZnONS)}_2 \qquad\qquad (3.1)$$

$$\text{(PRL–ZnONS)}_2 + \text{ PRL–ZnONS} \quad \rightarrow \text{ (PRL–ZnONS)}_3 \qquad\qquad (3.2)$$

$$\text{(PRL–ZnONS)}_3 + \text{ PRL–ZnONS} \quad \rightarrow \text{ (PRL–ZnONS)}_4 \qquad\qquad (3.3)$$

where PRL–ZnONS, (PRL–ZnONS)$_2$, (PRL–ZnONS)$_3$ and (PRL–ZnONS)$_4$ are single–, double–, triple– and quadruple–layer ZnOGLNSs, respectively. The stepwise ($\Delta E_{\text{binding}}^{\text{step}}$) and overall ($\Delta E_{\text{binding}}^{\text{overall}}$) binding energies are therefore defines by equations (3.4) and (3.7).

$$\Delta E_{\text{binding}}^{\text{step}} = E[(\text{PRL–ZnONS})_4] - \{E[(\text{PRL–ZnONS})_3] + E[\text{PRL–ZnONS}]\} \tag{3.4}$$

where $E[\text{PRL–ZnONS}]$, $E[(\text{PRL–ZnONS})_3]$ and $E[(\text{PRL–ZnONS})_4]$ are total energies of single–, triple– and quadruple–layer ZnOGLNSs, respectively.

For their overall binding processes are defined as equations (3.5) and (3.6).

$$3\ \text{PRL–ZnONS} \quad \rightarrow \quad (\text{PRL–ZnONS})_3 \tag{3.5}$$

$$4\ \text{PRL–ZnONS} \quad \rightarrow \quad (\text{PRL–ZnONS})_4 \tag{3.6}$$

Therefore,

$$\Delta E_{\text{binding}}^{\text{overall}} = E[(\text{PRL–ZnONS})_4] - 4\ E[\text{PRL–ZnONS}] \tag{3.7}$$

3.3 Adsorption of ammonia and water on CNL-ZnONS'

Adsorption energy (ΔE_{ads}) of adsorbate (NH$_3$ and H$_2$O) on CNL–ZnONS' and multiple–layer CNL–ZnONS's are defined by equations (3.8).

$$\Delta E_{\text{ads}} = E_{\text{adsorbate/CNL–ZnOGLNS'}} - (E_{\text{CNL–ZnOGLNS'}} + E_{\text{adsorbate}}) \tag{3.8}$$

where $E_{\text{adsorbate/CNL–ZnOGLNS'}}$, $E_{\text{CNL–ZnOGLNS'}}$ and $E_{\text{adsorbate}}$ are total energies of gas adsorption form, CNL–ZnOGLNS' sheet and isolated adsorbate, respectively.

Several chemical indices such as electronic chemical potential [μ] [58–59], chemical hardness [η] [60], global softness [S] [60–61] can measure the reactivity of molecular systems. These Chemical indices η and S are derived from local hardness [62–63], local softness [64] and Fukui function [65–66]. For the N electron molecular system with a total energy (E) and external potential ($\upsilon(\bar{r})$), μ and η can be computed

by equations: $\mu = \left(\dfrac{\partial E}{\partial N}\right)_{\upsilon(\bar{r})}$ and $\eta = \left(\dfrac{\partial^2 E}{\partial N^2}\right)_{\upsilon(\bar{r})}$ which can be approximate from the

ionization potential (*IP*) and electron affinity (*EA*) of the system as $\mu \approx -\dfrac{1}{2}(IP + EA)$

and $\eta \approx \dfrac{1}{2}(IP - EA)$, respectively. *S* can be computed by equation: $S \approx \dfrac{1}{(IP - EA)}$ or

$S = \dfrac{1}{2\eta}$. *IP* and *EA* can be computed from energies of the *N* (E_N) and *N±1* electron

(E_{N-1} and E_{N+1}) systems by equations: $IP = E_{N-1} - E_N$ and $EA = E_N - E_{N+1}$ [67].

Mulliken electronegativity (χ), electrophilicity (ω) and the maximum electronic charge transfer (ΔN_{max}) can be derived from μ and η as follows: $\chi = -\mu$,

$\omega = \dfrac{\mu^2}{2\eta}$ and $\Delta N_{max} = -\dfrac{\mu}{\eta}$ [68–69]. According to the Koopmans [70–73] theorem,

IP and *EA* were computed from the HOMO and LUMO energies using the relations: $IP = -E_{HOMO}$ and $EA = -E_{LUMO}$.
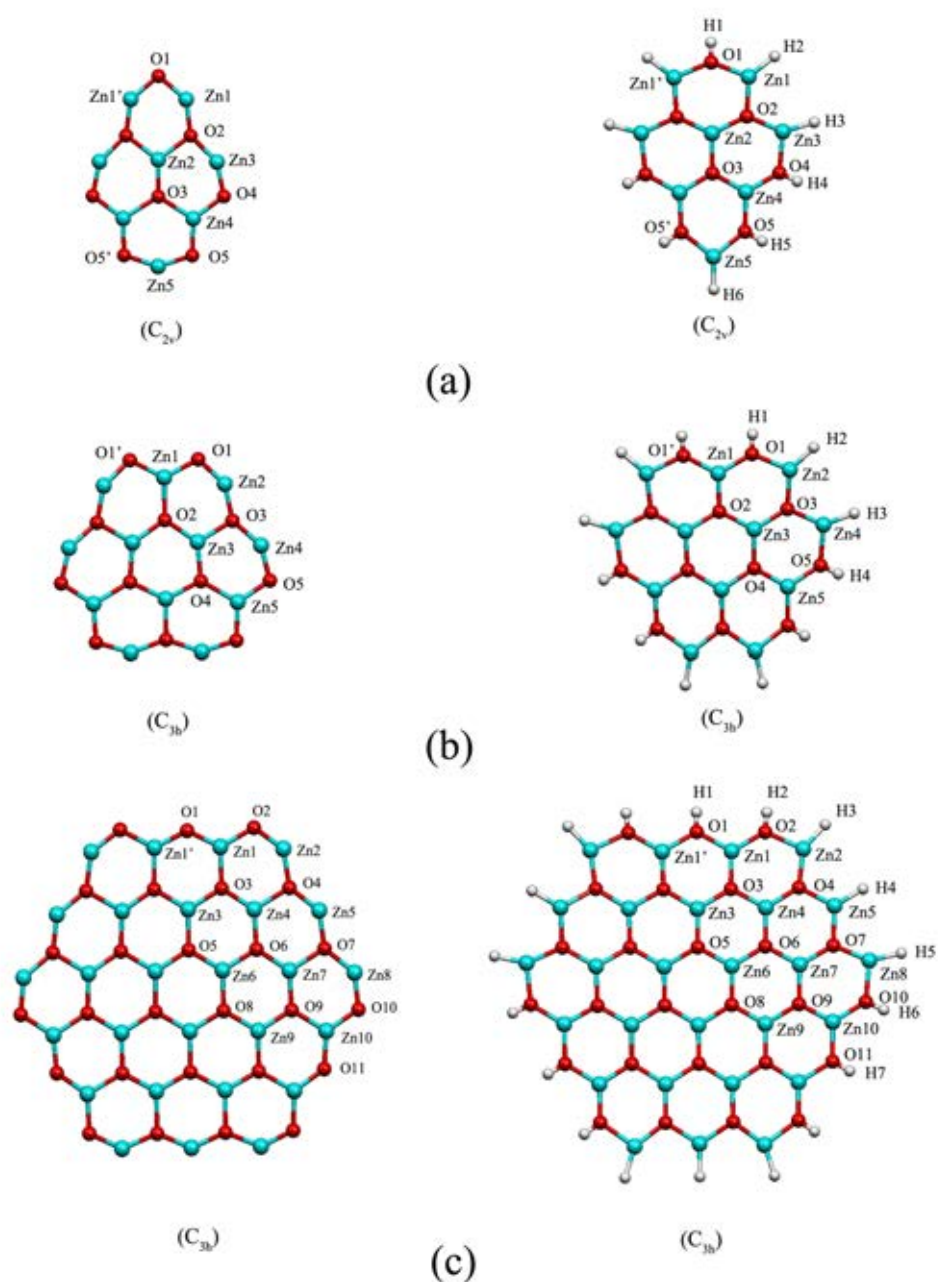
Figure 3.1 The B3LYP/LanL2DZ–optimized structures of the (a) PRL–ZnONS' (left), PRL–ZnONS (right), (b) CNL−ZnONS' (left), CNL−ZnONS (right) and (c) CCL−ZnONS' (left), CCL−ZnONS (right) nanosheets and their molecular symmetries are demonstrated. Atomic numberings for their representative atoms are defined.

CHAPTER IV

RESULTS AND DISCUSSION

4.1 Structures of ZnOGLNSs

The single−layer ZnOGLNS structures obtained from DFT optimizations at the B3LYP/LanL2DZ level. It shows Figure 4.1 non− and hydrogen−terminated nanosheets of ZnOGLNS namely of as PRL–ZnONS, CNL−ZnONS and CCL−ZnONS. These pairs of ZnOGLNSs structure are in the same symmetrical group but their hexagonal rings are differently distorted from the perfect ring.

4.1.1 PRL−ZnONS' and PRL−ZnONS

The optimized structures of single−layer PRL−ZnOGNS', double−layer (PRL−ZnOGNS')$_2$, triple−layer (PRL−ZnOGNS')$_3$, quadruple−layer (PRL−ZnOGNS')$_4$ for non−terminated forms and single−layer PRL−ZnOGNS, double−layer (PRL−ZnOGNS)$_2$, triple−layer (PRL−ZnOGNS)$_3$, quadruple−layer (PRL−ZnOGNS)$_4$ for hydrogen−terminated forms are shown in Figure 4.2. All interlayer distances (the shorted Zn$\cdots$O distance) for non−terminated forms of double−, triple− and quadruple−layer PRL−ZnOGNS are shorter than that of non−terminated forms. The reason is that repulsive interactions of hydrogen terminated atoms are taking place along the rim of cluster. The two interlayer distances (2.17 and 2.20 Å) for (PRL−ZnOGNS)$_3$, and three interlayer distances (2.12, 213 and 2.17 Å) for (PRL−ZnOGNS)$_4$ are not equal and not equivalent, see Figure 4.2(g) and 4.3(h).
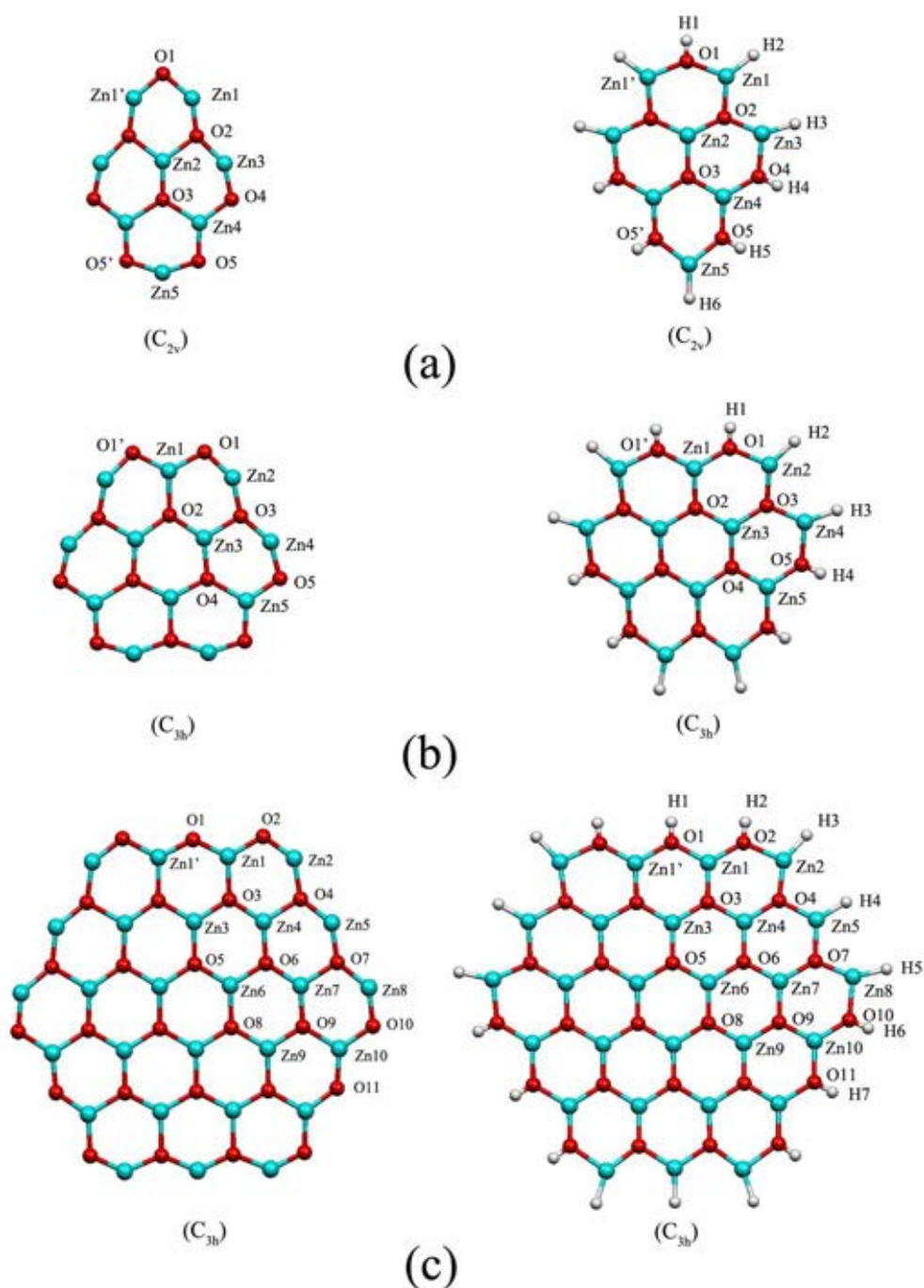
Figure 4.1 The B3LYP/LanL2DZ–optimized structures of single–layer (a) PRL–ZnONS' (left), PRL–ZnONS (right), (b) CNL–ZnONS' (left), CNL–ZnONS (right) and (c) CCL−ZnONS' (left), CCL−ZnONS (right) nanosheets and their molecular symmetries are demonstrated. Atomic numberings for their representative atoms are defined.
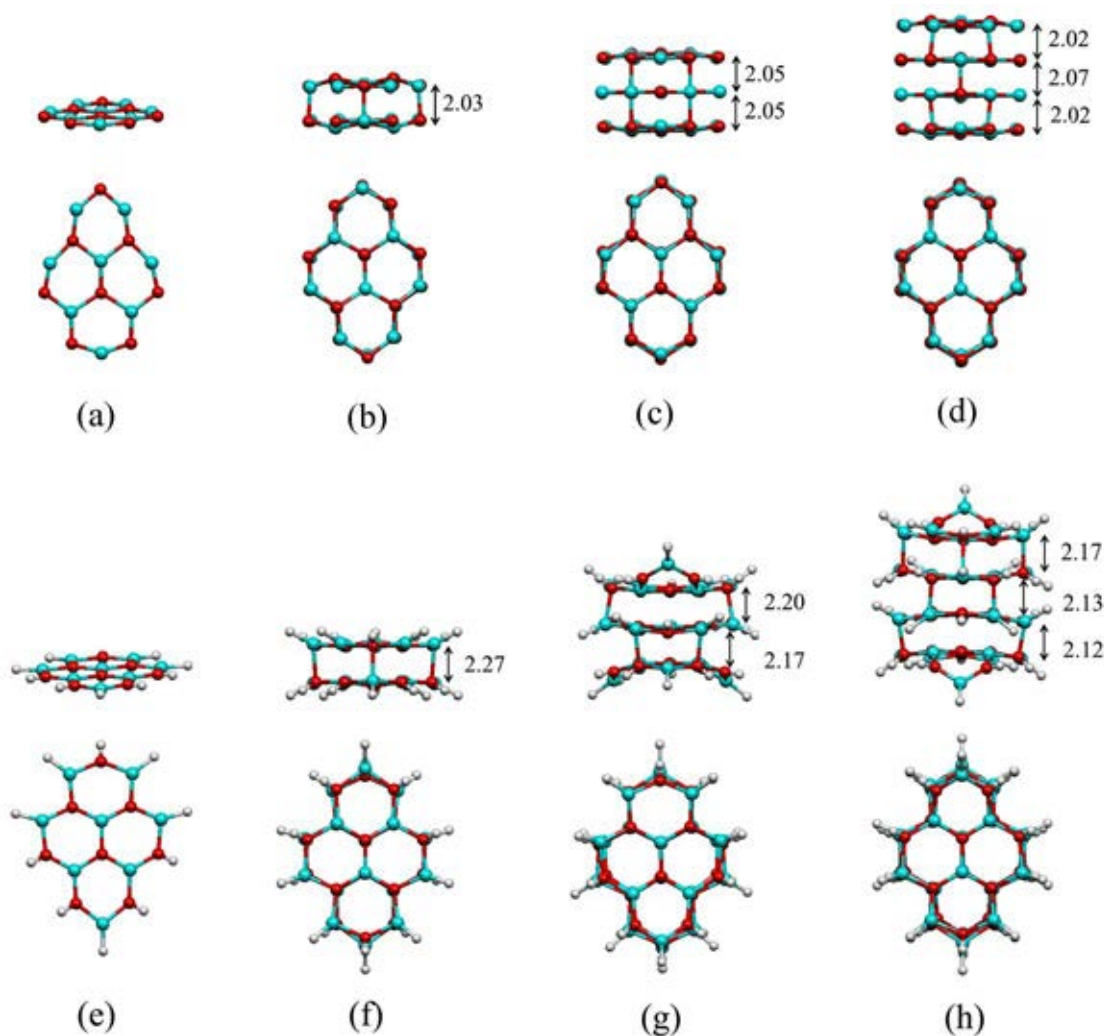
Figure 4.2 Optimized structures of (a) single−layer, PRL−ZnOGNS', (b) double−layer, (PRL−ZnOGNS')$_2$, (c) triple−layer, (PRL−ZnOGNS')$_3$, (d) quadruple−layer, (PRL−ZnOGNS')$_4$ for non−terminated forms, (e) single−layer, PRL−ZnOGNS, (f) double−layer, (PRL−ZnOGNS)$_2$, (g) triple−layer, (PRL−ZnOGNS)$_3$, (h) quadruple−layer, (PRL−ZnOGNS)$_4$ for hydrogen−terminated forms. Side (top) and top (bottom) views are shown. Bond distances are in Å.

4.1.2 CNL–ZnONS' and CNL–ZnONS

The optimized structures of single−layer CNL−ZnOGNS', double−layer (CNL−ZnOGNS')$_2$, triple−layer (CNL−ZnOGNS')$_3$, quadruple−layer (CNL−ZnOGNS')$_4$ for non−terminated forms and single−layer CNL−ZnOGNS, double−layer (CNL−ZnOGNS)$_2$, triple−layer (CNL−ZnOGNS)$_3$, quadruple−layer (CNL−ZnOGNS)$_4$ for hydrogen−terminated forms are shown in Figure 4.3. All interlayer distances for non−terminated forms of double−, triple− and quadruple−layer CNL−ZnOGNS are much shorter than that of non−terminated corresponding forms. The two interlayer distances (2.25 and 2.65 Å) for (CNL−ZnOGNS)$_3$, and three interlayer distances (2.14, 2.84 and 2.18 Å) for (CNL−ZnOGNS)$_4$ are not equal and not equivalent, see Figure 4.3(g) and 4.3(h).

4.1.3 CCL–ZnONS' and CCL–ZnONS

The optimized structures of single−layer CCL−ZnOGNS', double−layer (CCL−ZnOGNS')$_2$, triple−layer (CCL−ZnOGNS')$_3$, quadruple−layer, (CCL−ZnOGNS')$_4$ for non−terminated forms, single−layer CCL−ZnOGNS and double−layer (CCL−ZnOGNS)$_2$, for hydrogen−terminated forms are shown in Figure 4.4. Only double−layer (CCL−ZnOGNS)$_2$ which has interlayer distance was obtained. The interlayer distance for (CCL−ZnOGNS)$_2$ is slightly shorter than (CCL−ZnOGNS')$_2$. Triple−layer (CCL−ZnOGNS)$_3$ and quadruple−layer, (CCL−ZnOGNS)$_4$ seem to be not quite stable and their structure optimizations are therefore not carried out.

Nevertheless, interlayer distances of each non–terminated double−layer, triple−layer, quadruple−layer for either PRL−ZnOGNS or CNL−ZnOGNS or CCL−ZnOGNS are quite equal and equivalent. Plots of hydrogenation energies (per molecule of H$_2$) of ZnONS's against their layer numbers for PRL−ZnONS', CNL−ZnONS' and CCL−ZnONS' are shown in Figure 4.5. It shows that hydrogenation energies of ZnONS's are decreased when numbers of their layers are increased. Thus, hydrogenation energies for large layer numbers of ZnONS's may be converted to a single value.
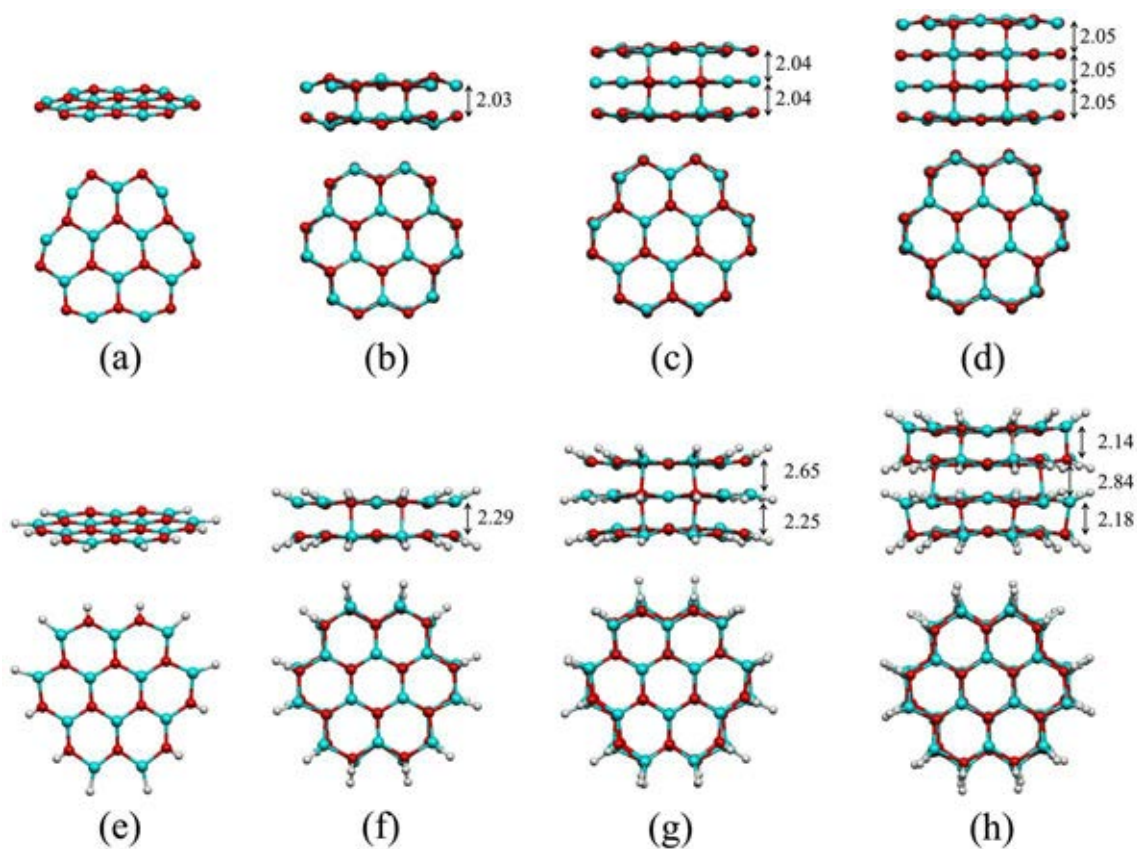
Figure 4.3 Optimized structures of (a) single−layer, CNL−ZnOGNS', (b) double−layer, (CNL−ZnOGNS')$_2$, (c) triple−layer, (CNL−ZnOGNS')$_3$, (d) quadruple−layer, (CNL−ZnOGNS')$_4$ for non−terminated forms, (e) single−layer, CNL−ZnOGNS, (f) double−layer, (CNL−ZnOGNS)$_2$, (g) triple−layer, (CNL−ZnOGNS)$_3$, (h) quadruple−layer, (CNL−ZnOGNS)$_4$ for hydrogen−terminated forms. Side (top) and top (bottom) views are shown. Bond distances are in Å.
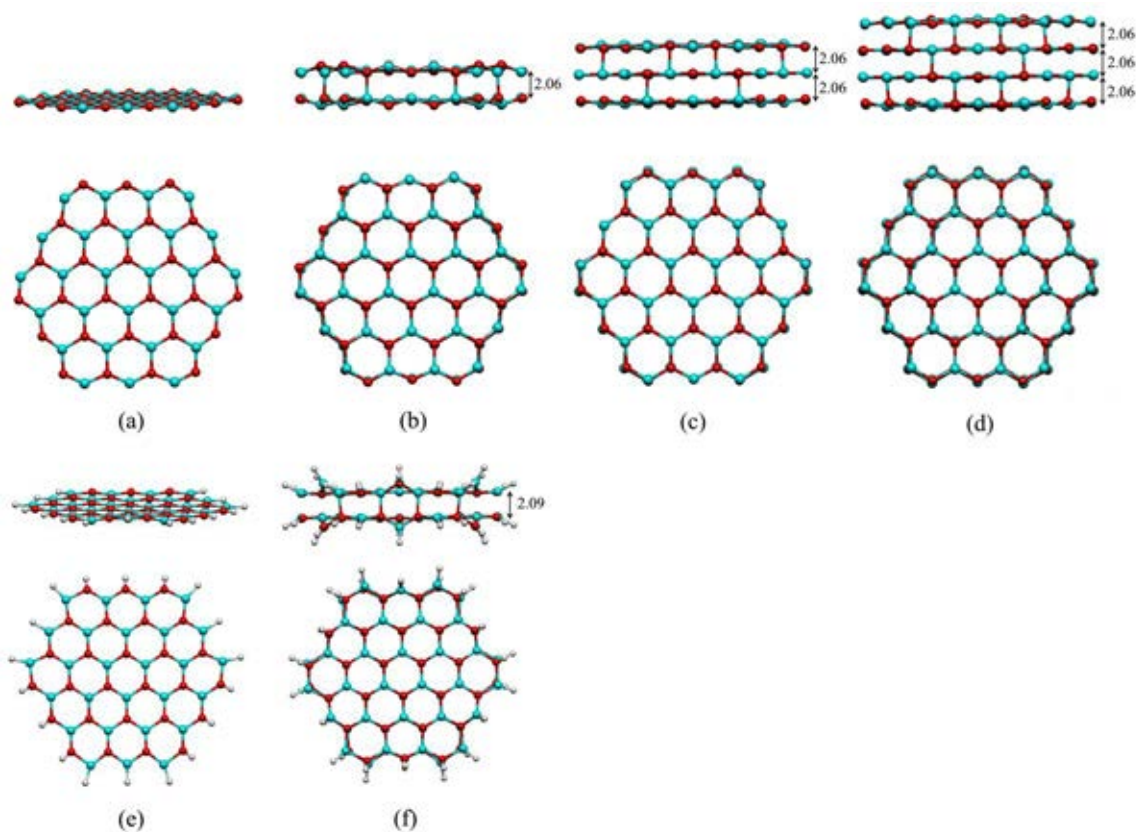
Figure 4.4 Optimized structures of (a) single−layer, CCL−ZnOGNS', (b) double−layer, (CCL−ZnOGNS')$_2$, (c) triple−layer, (CCL−ZnOGNS')$_3$, (d) quadruple−layer, (CCL−ZnOGNS')$_4$ for non−terminated forms, (e) single−layer, CCL−ZnOGNS, (f) double−layer (CCL−ZnOGNS)$_2$, for hydrogen−terminated forms. Side (top) and top (bottom) views are shown. Bond distances are in Å.
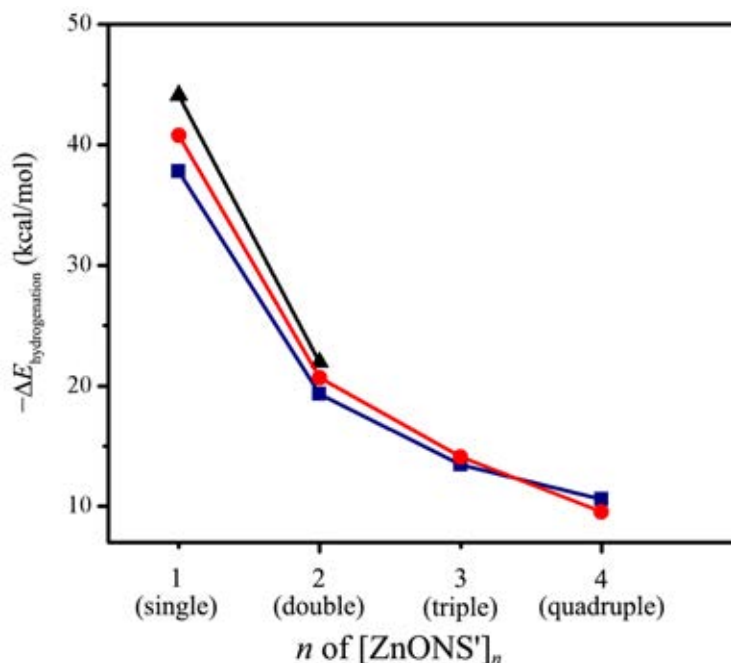
Figure 4.5 Plots of hydrogenation energies (per molecule of H_2) of ZnONS's against their layer numbers for PRL−ZnONS' (■), CNL−ZnONS' (●), and CCL−ZnONS' (▲).

4.2 Binding energies for multi–layerizations

Binding energies for multi–layerization of non–terminated ZnO graphene–like nanosheets (ZnOGLNS's) are shown in Table 4.1. The stepwise binding energies ($\Delta E_{binding}^{step}$) of PRL–ZnONS's, CNL–ZnONS's and CCL–ZnONS's systems are the same sequences and their 1st:2nd:3rd ratios are −332.23:−287.47:−322.03,−402.89:−360.39:−390.83 and −848.16:−507.12:−779.76, respectively. The 1st, 2nd and 3rd stepwise binding energies for ZnONS's systems are in the same orders: PRL–ZnONS' (−332.23 kcal/mol) >CNL–ZnONS' (−402.89 kcal/mol) > CCL–ZnONS' (−848.16 kcal/mol), PRL–ZnONS' (−287.47 kcal/mol) >CNL–ZnONS' (−360.39 kcal/mol) > CCL–ZnONS' (−507.12 kcal/mol) and PRL–ZnONS' (−322.03 kcal/mol) >CNL–ZnONS' (−390.83 kcal/mol) > CCL–ZnONS' (−779.76 kcal/mol), respectively.

Table 4.1 Binding energies for multi–layerization of non–terminated ZnO graphene–like nanosheets (ZnOGLNS's).

Reactions	$\Delta E_{binding}^{step}$ [a,b]	$\Delta E_{binding}^{overall}$ [a,c]
Pyrene–like system:		
2 PRL–ZnONS' → (PRL–ZnONS')$_2$	−332.23	−332.23
(PRL–ZnONS')$_2$ + PRL–ZnONS' → (PRL–ZnONS')$_3$	−287.47	−619.69
(PRL–ZnONS')$_3$ + PRL–ZnONS' → (PRL–ZnONS')$_4$	−322.03	−941.72
Coronene–like system:		
2 CNL–ZnONS' → (CNL–ZnONS')$_2$	−402.89	−402.89
(CNL–ZnONS')$_2$ + CNL–ZnONS' → (CNL–ZnONS')$_3$	−360.39	−763.28
(CNL–ZnONS')$_3$ + CNL–ZnONS' → (CNL–ZnONS')$_4$	−390.83	−1154.10
Circumcoronene–like system:		
2CCL–ZnONS' → (CCL–ZnONS')$_2$	−848.16	−848.16
(CCL–ZnONS')$_2$ + CCL–ZnONS' → (CCL–ZnONS')$_3$	−507.12	−1406.95
(CCL–ZnONS')$_3$ + CCL–ZnONS' → (CCL–ZnONS')$_4$	−779.76	−2186.71

[a] Computed at B3LYP/LanL2DZ level, in kcal/mol.

[b] Stepwise binding energy.

[c] Overall binding energy.

Binding energies for multi–layerization of hydrogen–terminated ZnO graphene–like nanosheets (ZnOGLNSs) are shown in Table 4.2. The stepwise binding energies of PRL–ZnONSs and CNL–ZnONSs systems are the same sequences and their 1st:2nd:3rd ratios are −134.37:−89.49:−99.11 and −181.67:−143.74:−176.35, respectively. As structures of (CCL–ZnONS)$_3$ and (CCL–ZnONS) are no existing, no the 2nd and 3rd stepwise binding energies of CCL–ZnONSs system is obtained.

Nevertheless, the 1st stepwise binding energies for PRL–ZnONS, CNL–ZnONS and CCL–ZnONS are in the same order: PRL–ZnONS (–134.37 kcal/mol) >CNL– ZnONS' (–181.67 kcal/mol) > CCL–ZnONS' (–449.26 kcal/mol) which are the same orders of all non–terminated ZnOGLNS's.

Table 4.2 Binding energies for multi–layerization of hydrogen–terminated ZnO graphene– like nanosheets (ZnOGLNSs).

Reactions	$\Delta E_{binding}^{step}$ [a,b]	$\Delta E_{binding}^{overall}$ [a,c]
Pyrene–like system:		
2 PRL–ZnONS $\rightarrow$ (PRL–ZnONS)$_2$	–134.37	–134.37
(PRL–ZnONS)$_2$ + PRL–ZnONS $\rightarrow$ (PRL–ZnONS)$_3$	–89.49	–223.86
(PRL–ZnONS)$_3$ + PRL–ZnONS $\rightarrow$ (PRL–ZnONS)$_4$	–99.11	–322.97
Coronene–like system:		
2 CNL–ZnONS $\rightarrow$ (CNL–ZnONS)$_2$	–181.67	–181.67
(CNL–ZnONS)$_2$ + CNL–ZnONS $\rightarrow$ (CNL–ZnONS)$_3$	–143.74	–325.41
(CNL–ZnONS)$_3$ + CNL–ZnONS $\rightarrow$ (CNL–ZnONS)$_4$	–176.35	–501.77
Circumcoronene–like system:		
2 CCL–ZnONS $\rightarrow$ (CCL–ZnONS)$_2$	–449.26	–449.26
(CCL–ZnONS)$_2$ + CCL–ZnONS $\rightarrow$ (CCL–ZnONS)$_3$	–[d]	–[d]
(CCL–ZnONS)$_3$ + CCL–ZnONS $\rightarrow$ (CCL–ZnONS)$_4$	–[e]	–[e]

[a] Computed at B3LYP/LanL2DZ level, in kcal/mol.

[b] Stepwise binding energy.

[c] Overall binding energy.

[d] No B3LYP/LanL2DZ–optimized structure of (CCL–ZnONS)$_3$ is carried out.

[e] No B3LYP/LanL2DZ–optimized structure of (CCL–ZnONS)$_4$ is carried out

4.3 Hydrogenations of ZnOGLNS's

Hydrogenations of ZnO graphene–like nanosheets to form multi–layer nanosheets and their corresponding energies are shown in Table 4.3. Hydrogenation energies of PRL–ZnOGLNS's, are in the same orders: PRL–ZnONS' –40.48 kcal/mol < (PRL–ZnONS')$_2$ –20.69 kcal/mol < (PRL–ZnONS')$_3$ –14.09 kcal/mol < (PRL–ZnONS')$_4$ –9.54 kcal/mol , CNL–ZnONS' –37.78 kcal/mol < (CNL–ZnONS')$_2$ –19.33 kcal/mol < (CNL–ZnONS')$_3$ –13.45 kcal/mol < (CNL–ZnONS')$_4$ –10.60 kcal/mol and CCL–ZnONS' –44.11 kcal/mol < (CCL–ZnONS')$_2$ –21.94 kcal/mol, respectively. As numbers of hydrogen molecules per one layer of PRL–ZnONS's, CNL–ZnONS's and CCL–ZnONS's systems are 5, 6 and 9, respectively, therefore hydrogen molecules weight–percentage uptake unit of these clusters are in order: PRL–ZnONS's (1.55%) > CNL–ZnONS's (1.24%) > CCL–ZnONS's (0.83%).

Table 4.3 Hydrogenations of ZnO graphene–like nanosheets to form multi–layer nanosheets and their corresponding energies.

Reactions/systems	$\Delta E_{hydrogenation}^{overall}$ [a]	$\Delta E_{hydrogenation}$ [b]
Pyrene–like system:		
PRL–ZnONS' + 5H$_2$ → PRL–ZnONS	−202.40	−40.48
(PRL–ZnONS')$_2$ + 10H$_2$ → (PRL–ZnONS)$_2$	−206.94	−20.69
(PRL–ZnONS')$_3$ + 15H$_2$ → (PRL–ZnONS)$_3$	−211.36	−14.09
(PRL–ZnONS')$_4$ + 20H$_2$ → (PRL–ZnONS)$_4$	−190.83	−9.54
Coronene–like system:		
CNL–ZnONS' + 6H$_2$ → CNL–ZnONS	−226.68	−37.78
(CNL–ZnONS')$_2$ + 12H$_2$ → (CNL–ZnONS)$_2$	−232.15	−19.33
(CNL–ZnONS')$_3$ + 18H$_2$ → (CNL–ZnONS)$_3$	−242.18	−13.45
(CNL–ZnONS')$_4$ + 24H$_2$ → (CNL–ZnONS)$_4$	−254.39	−10.60
Circumcoronene–like system:		
CCL–ZnONS' + 9H$_2$ → CCL–ZnONS	−396.95	−44.11
(CCL–ZnONS')$_2$ + 18H$_2$ → (CCL–ZnONS)$_2$	−395.01	−21.94
(CCL–ZnONS')$_3$ + 27H$_2$ → (CCL–ZnONS)$_3$	−	−
(CCL–ZnONS')$_4$ + 36H$_2$ → (CCL–ZnONS)$_4$	−	−

[a] In kcal/mol.

[b] In kcal/mol per hydrogen molecule.

4.4 Energy gaps and chemical indices of ZnOGLNS's and ZnOGLNSs

Orbital energies, HOMOs, LUMOs, energy gaps and chemical indices of non–(ZnONS's) and hydrogen–terminated ZnO graphene–like (ZnONSs) nanosheets and nanosheets are shown in Table 4.4. In all cases, energy gaps of each ZnONS's are lower than their corresponding hydrogen–terminated nanosheets by at least 0.52 eV as shown in Figure 4.6. Figure 4.6 shows also plots of orbital energies, HOMOs and LUMOs of ZnONS's against their layer numbers (n) for PRL−ZnONS', PRL−ZnONS, CNL−ZnONS', CNL−ZnONS, CCL−ZnONS' and CCL−ZnONS. It means that all terminal hydrogen atoms cause reduction of reactivity of hydrogen–terminated nanosheets. The electrophilicity indices for single layer non–terminated nanosheets are remarkably high as ω[PRL–ZnONS'] = 25.71 eV, ω[CNL–ZnONS'] = 7.34 eV and ω[CCL–ZnONS'] = 46.40 eV. This indicates that electron changes on these nanosheets are large.

Table 4.4 Orbital energies, HOMOs, LUMOs, energy gaps (in eV) and chemical indices of non– and hydrogen–terminated ZnO graphene–like nanosheets.

Species	E_{LUMO}[a]	E_{HOMO}[a]	E_{gap}[a]	η[b]	μ[c]	χ[d]	ω[e]
Pyrene–like system:							
PRL–ZnONS'	−4.36	−5.26	0.90	0.45	−4.81	4.81	25.71
(PRL–ZnONS')$_2$	−3.09	−6.50	3.41	1.71	−4.80	4.80	6.74
(PRL–ZnONS')$_3$	−3.55	−5.69	2.14	1.07	−4.62	4.62	9.97
(PRL–ZnONS')$_4$	−3.13	−6.27	3.14	1.57	−4.70	4.70	7.04
PRL–ZnONS	−2.21	−6.47	4.26	2.13	−4.34	4.34	4.42
(PRL–ZnONS)$_2$	−2.58	−7.12	4.54	2.27	−4.85	4.85	5.18
(PRL–ZnONS)$_3$	−2.71	−7.00	4.29	2.15	−4.86	4.86	5.49
(PRL–ZnONS)$_4$	−2.74	−7.33	4.59	2.30	−5.04	5.04	5.52
Coronene–like system:							
CNL–ZnONS'	−3.27	−6.56	3.29	1.65	−4.92	4.92	7.34
(CNL–ZnONS')$_2$	−3.08	−6.52	3.44	1.72	−4.80	4.80	6.70
(CNL–ZnONS')$_3$	−3.15	−6.36	3.21	1.61	−4.76	4.76	7.04
(CNL–ZnONS')$_4$	−3.10	−6.40	3.30	1.65	−4.75	4.75	6.84
CNL–ZnONS	−2.14	−6.98	4.84	2.42	−4.56	4.56	4.30
(CNL–ZnONS)$_2$	−2.81	−7.11	4.30	2.15	−4.96	4.96	5.72
(CNL–ZnONS)$_3$	−3.00	−7.17	4.17	2.09	−5.09	5.09	6.20
(CNL–ZnONS)$_4$	−3.13	−7.32	4.19	2.10	−5.23	5.23	6.52
Circumcoronene–like system:							
CCL–ZnONS'	−4.49	−4.97	0.48	0.24	−4.73	0.24	46.40
(CCL–ZnONS')$_2$	−3.05	−6.54	3.53	1.77	−4.78	4.78	6.46
(CCL–ZnONS')$_3$	−3.48	−5.76	2.28	1.14	−4.62	1.14	9.38
(CCL–ZnONS')$_4$	_[f]	_[f]	_[f]	_[f]	_[f]	_[f]	_[f]
CCL–ZnONS	−2.54	−6.29	3.75	1.88	−4.42	4.42	5.20
(CCL–ZnONS)$_2$	−3.02	−7.07	4.05	2.03	−5.05	5.05	6.28
(CCL–ZnONS)$_3$	_[g]	_[g]	_[g]	_[g]	_[g]	_[g]	_[g]
(CCL–ZnONS)$_4$	_[h]	_[h]	_[h]	_[h]	_[h]	_[h]	_[h]

[a] In eV.

[b] Chemical hardness, $\eta = E_{gap}/2$.

[c] Electronic chemical potential, $\mu = (E_{HOMO} + E_{LUMO})/2$.

[d] The Mulliken electronegativity index, $\chi = -(E_{HOMO} + E_{LUMO})/2$.

[e] The electrophilicity index, $\omega = \mu^2/2\eta$

[g] No B3LYP/LanL2DZ optimized structure of (CCL–ZnONS)$_3$ is carried out.

[h] No B3LYP/LanL2DZ optimized structure of (CCL–ZnONS)$_4$ is carried out.
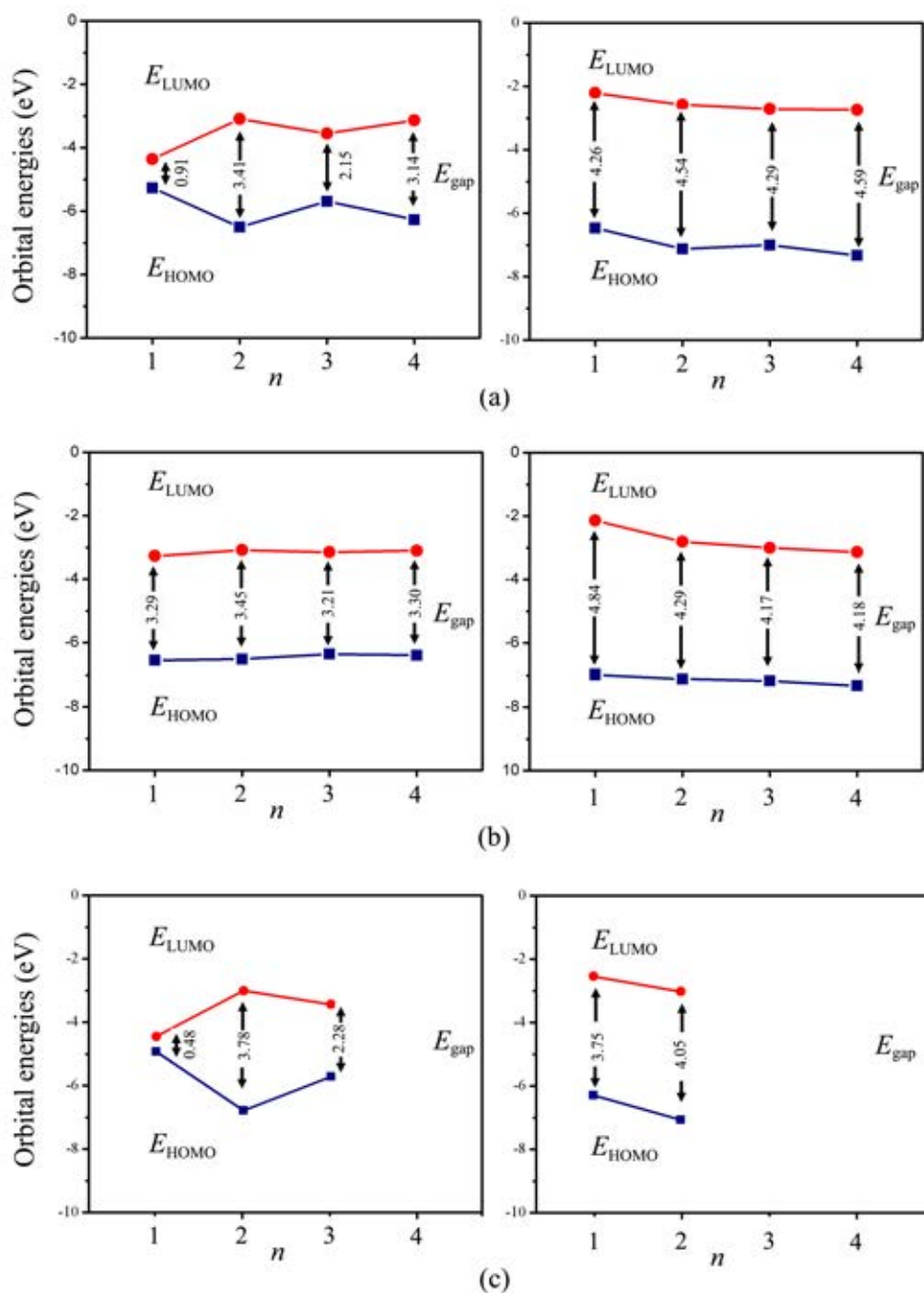
Figure 4.6 Plots of orbital energies (HOMOs and LUMOs) of ZnONSs against their layer numbers (*n*) for (a) PRL−ZnONS' (left) and PRL−ZnONS (right), (b) CNL−ZnONS' (left) and CNL−ZnONS (right) and (c) CCL−ZnONS' (left) and CCL−ZnONS (right). Their energy gaps (E_{gap}) are indicated.

4.5 Adsorption of molecule gaseous on CNL-ZnOS' nanosheets

4.5.1 Structures of CNL–ZnONS' and its multiple sheets

The B3LYP/LanL2DZ–optimized structures of the CNL–ZnONS' and its double–, triple– and quadruple–layer species were obtained as shown in Figure 4.7. Energy gaps for the single–, double–, triple– and quadruple–layer CNL–ZnONS's are 3.29, 3.44, 3.21 and 3.30 eV, respectively and plot of their energy gaps of related with values of their layers (n) is shown in Figure 4.8. It seems to be that the odd layer numbers of CNL–ZnONS's clusters are less value than the next even layer number. This may suggest that odd–layer clusters trends to more reactive than their next even–layer clusters. It can predict that either odd– or even–layer cluster at high layer–number may approach to single value which is the lowest value of energy gap.

$E_{gap} = 3.290$ eV
(a)

$E_{gap} = 3.447$ eV
(b)

$E_{gap} = 3.210$ eV
(c)

$E_{gap} = 3.300$ eV
(d)
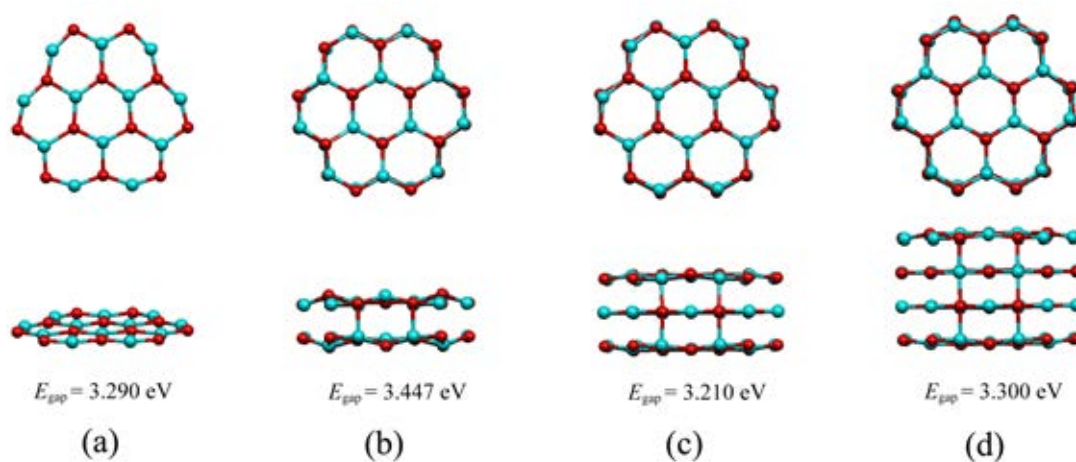
Figure 4.7 The B3LYP/LanL2DZ–optimized structures of (a) single–, (b) double–, (c) triple– and (d) quadruple–layer CNL–ZnONS's. Top and side views are at top and bottom, respectively.

4.5.1.1 Energy gap

The energy gap of multilayer of CNL-ZnONS's were shown in Figure 4.8.
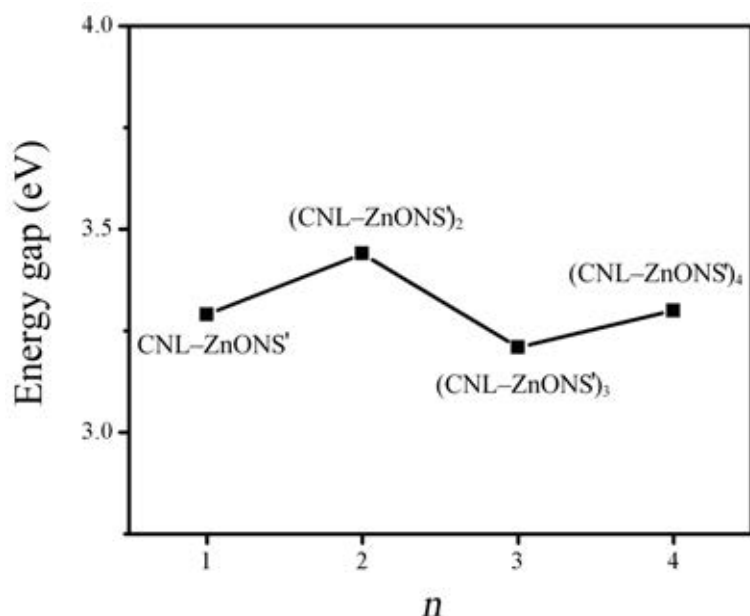
Figure 4.8 Plot of energy gaps of CNL-ZnONS' nanosheets against of their layers (*N*).

4.5.1.2 Atomic charge distribution

NBO charges (in e) on single–, double–, triple– and quadruple–layer CNL–ZnONS's are shown in Figure 4.9. The average partial charges for Zn (q_{Zn}) and O (q_O) atoms in hexagonal at the center of CNL–ZnONS's are $q_{Zn} = 1.63$ e, $q_O = -1.65$ e for single–layer and $q_{Zn} = 1.67$ e, $q_O = -1.68$ e for double–layer, respectively. The average partial charges of triple–layer CNL–ZnONS's are ($q_{Zn} = 1.68$ e, $q_O = -1.67$ e) for the outer (the first and third) layers and ($q_{Zn} = 1.65$ e, $q_O = -1.71$ e) for the middle (the second) layer, respectively. The average partial charges of quadruple–layer CNL–ZnONS's are ($q_{Zn} = 1.68$ e, $q_O = -1.66$ e) for the outer (the first and forth) layers and ($q_{Zn} = 1.66$ e, $q_O = -1.71$ e) for two middle (the second and third) layers, respectively. Charges for Zn and O atoms in each layer of various CNL–ZnONS' clusters are not homogeneously distributed.
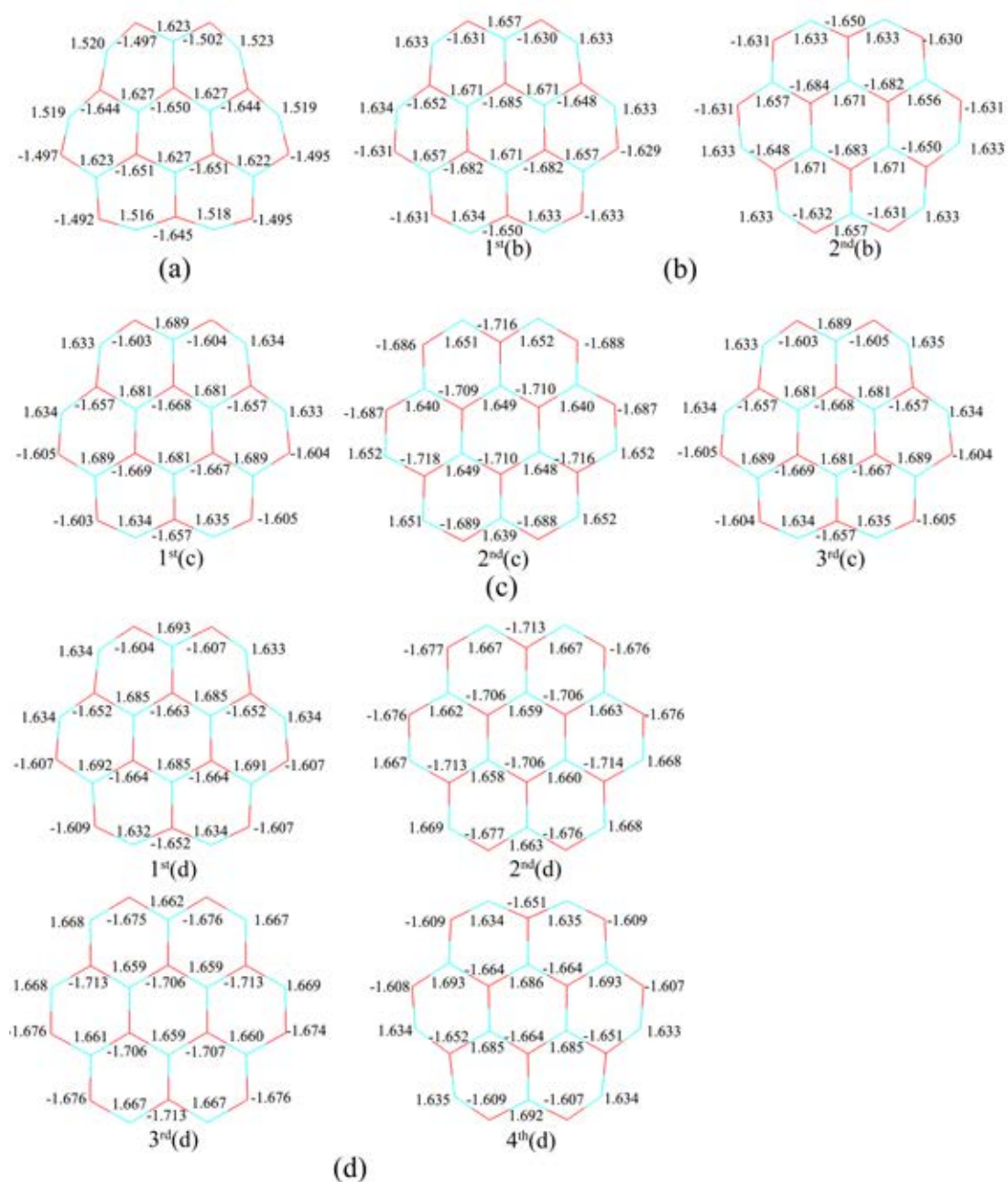
Figure 4.9 NBO charges (in e) on atoms in (a) single–, (b) double–, (c) triple– and (d) quadruple–layer CNL–ZnONS's. The layer numbers for each cluster are specified.

4.5.1.3 Energies of HOMO and LUMO orbitals

The B3LYP/LanL2DZ–energies of HOMO and LUMO orbitals of single–, double–, triple– and quadruple–layer CNL–ZnONS's and their density of state are shown in Figure 4.10. The HOMOs of single–layer CNL–ZnONS' are located over atoms at layer edge but LUMOs are somewhat located on both sides of the layer plane. The HOMOs and LUMOs of multi–layer CNL–ZnONS's are quite similar which HOMOs and LUMOs are located over atoms at layer edge.
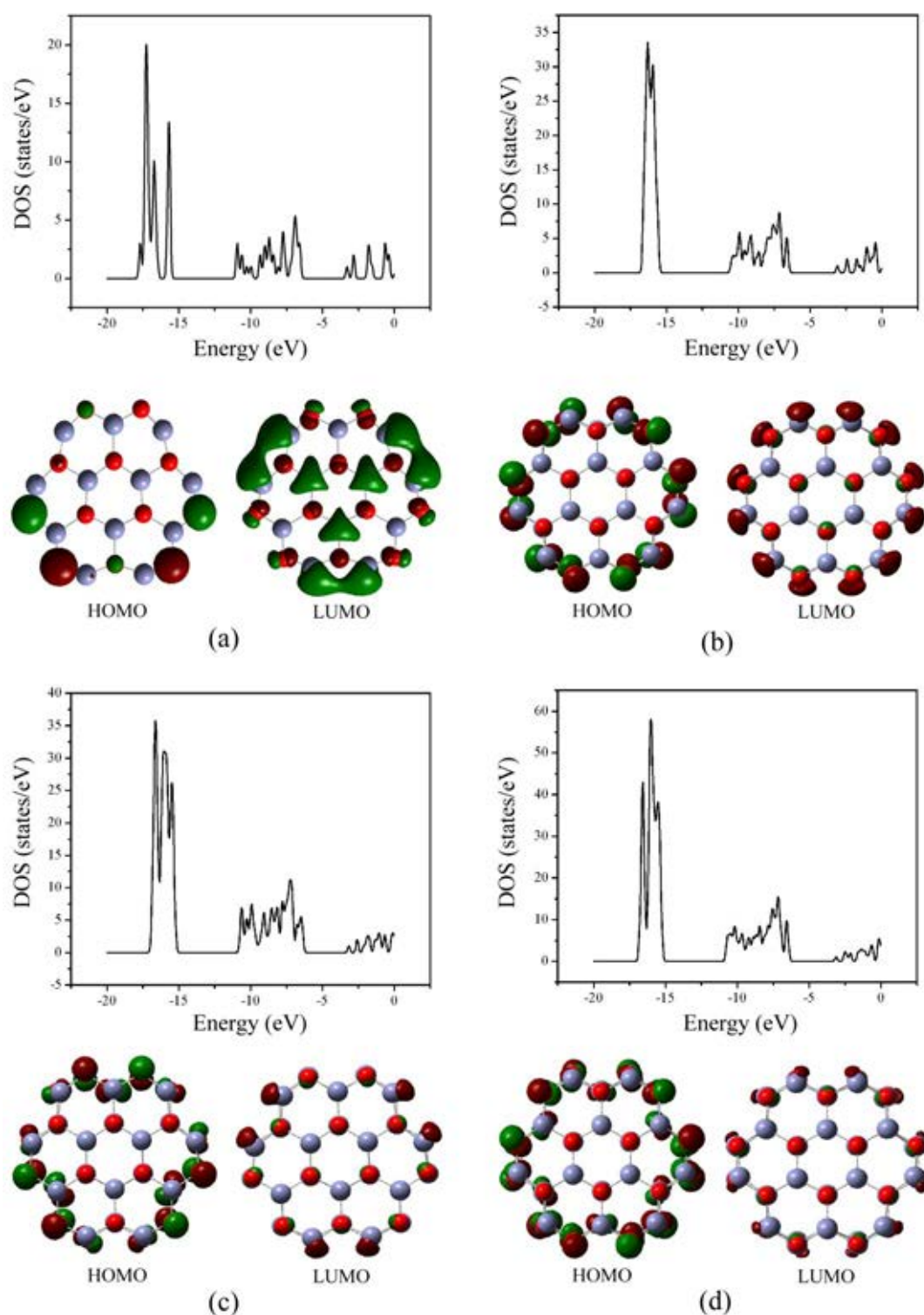
Figure 4.10 B3LYP/LanL2DZ–energies of HOMO and LUMO orbitals of (a) single, (b) double–, (c) triple– and (d) quadruple–layer CNL–ZnONS's and their density of state, located on their top.

4.5.2 Adsorption of ammonia molecule

The B3LYP/LanL2DZ–optimized structures of adsorption configurations of NH_3 on single– and multi–layer CNL–ZnONS's are shown in Figure 4.11 and their adsorption energies are shown in Table 4.5. The adsorption configurations of NH_3 adsorption on the single–, double–, triple– and quadruple–layer CNL–ZnONS's are composed of two configurations for each. All adsorption configurations are non–dissociative adsorption except one of the NH_3 on the single–layer CNL–ZnON'S which is dissociative. There are two types of NH_3 adsorptions on multi–layer CNL–ZnONS's. One adsorption site is at edge of outer layers and another is in between outer and the next inner layers. The adsorption energies of NH_3 on the edge of outer layer are slightly higher than of the inner layer. Their adsorption energies are within the range of –28.25 to –21.52 kcal/mol.
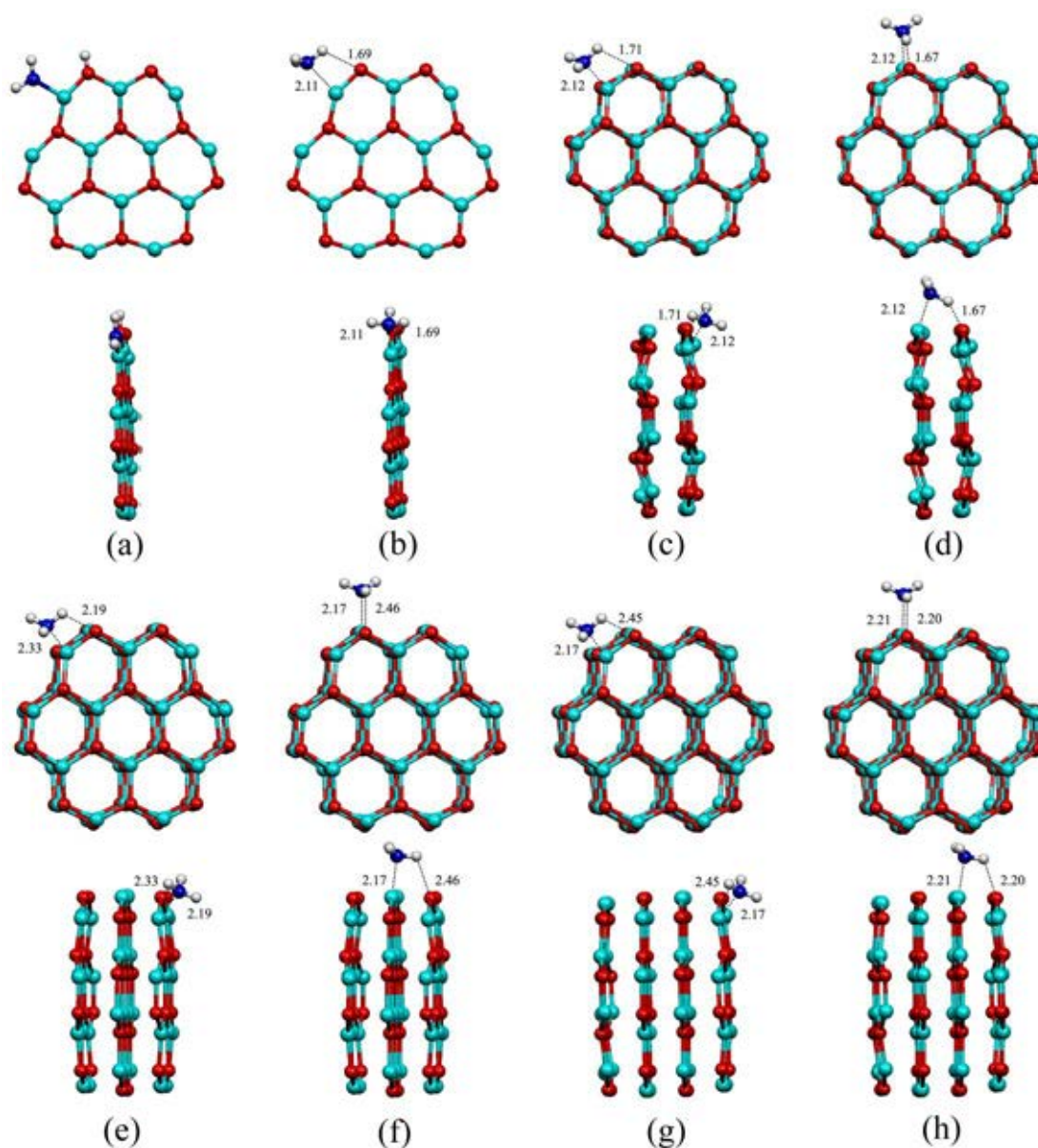
Figure 4.11 B3LYP/LanL2DZ–optimized structures of ammonia adsorption on CNL–ZnONS's as (a) H.NH$_2$/CNL–ZnONS' (1), (b) NH$_3$/CNL–ZnONS' (2), (c) NH$_3$/(CNL–ZnONS')$_2$ (1), (d) NH$_3$/(CNL–ZnONS')$_2$ (2), (e) NH$_3$/(CNL–ZnONS')$_3$ (1), (f) NH$_3$/(CNL–ZnONS')$_3$ (2), (g) NH$_3$/(CNL–ZnONS')$_4$ (1) and (h) NH$_3$/(CNL–ZnONS')$_4$ (2). Top and side views are shown on top and bottom, respectively. Bond distances are in Å.

4.5.3 Adsorption of water molecule

The optimized structures of adsorption configurations of water on single– and multi–layer CNL–ZnONS's are shown in Figure 4.12 and their adsorption energies are shown in Table 4.5. The adsorption configurations of water adsorption on the single–, double–, triple– and quadruple–layer CNL–ZnONS's are composed of two, two, three and four configurations, respectively. The adsorption energies of water on the single– layer CNL–ZnONS' are –40.18 kcal/mol for dissociative adsorption and –28.52 kcal/mol for non–dissociative adsorption. The adsorption energies for two adsorption configurations of water on double–layer CNL–ZnONS' are –27.04 kcal/mol at the edge within two layers and –28.24 kcal/mol at edge of outer layer. Three adsorption configurations of water on triple–layer CNL–ZnONS' are one dissociative and two non–dissociative adsorptions. The first two adsorption configurations, water molecules are located at the edge of outer layer and the third configuration, water is located at the edge within outer and the first inner layers. For water adsorption on the quadruple–layer CNL–ZnONS', two adsorption configurations of which water molecules are located at the edge of outer layer were found and their adsorption energies are –30.01 and –29.12 kcal/mol. For adsorption energies of water adsorption configurations of which water molecules are located at the edge within outer and the first inner layers and within the first and the second inner layers are –12.03 and – 13.72 kcal/mol, respectively. It can be concluded that the adsorption abilities of water adsorption on multiple–layer CNL–ZnONS's at the edge of outer layer are higher than their inner layers. The water adsorptions on the single–, triple– and quadruple–layer CNL–ZnONS's at the edge of outer layer were found to be dissociative adsorptions of which adsorption energies are –40.18, –30.24 and –30.01 kcal/mol, respectively.
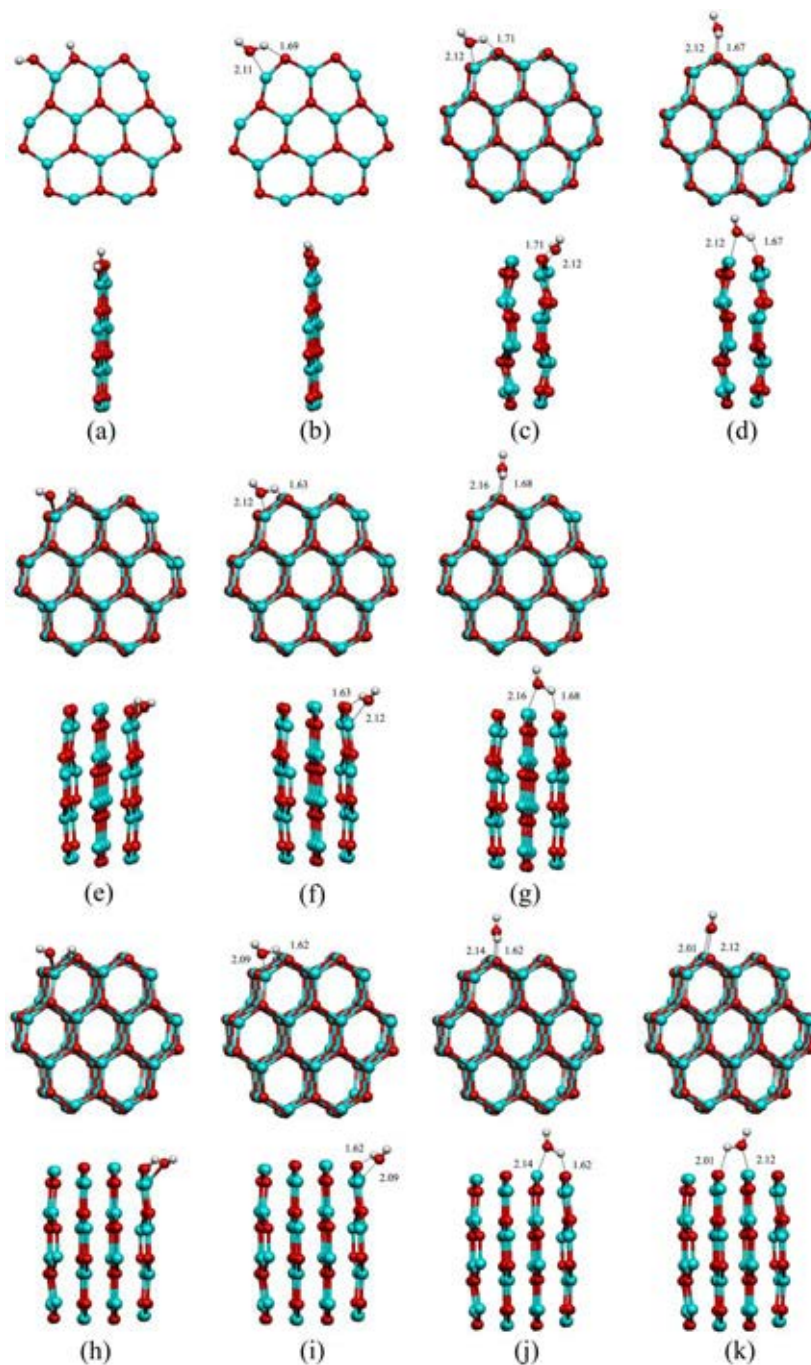
Figure 4.12 B3LYP/LanL2DZ–optimized structures of water adsorption on CNL–ZnONS's as (a) H.OH/CNL–ZnON'S (1), (b) H_2O/CNL–ZnON'S (2), (c) H_2O/(CNL–ZnONS')$_2$ (1), (d) H_2O/(CNL–ZnONS')$_2$ (2), (e) H.OH/(CNL–ZnONS')$_3$ (1), (f) H_2O/(CNL–ZnONS')$_3$ (2), (g) H_2O/(CNL–ZnONS')$_3$ (3), (h) H_2O/(CNL–ZnONS')$_4$ (1), (i) H_2O/(CNL–ZnONS')$_4$ (2), (j) H_2O/(CNL–ZnONS')$_4$ (3) and (k) H_2O/(CNL–ZnONS')$_4$ (4). Top and side views are shown on top and bottom, respectively. Bond distances are in Å.

4.5.4 Energy gaps and chemical indices of adsorption complexes with CNL–ZnONS's

The energy gaps, chemical indices and electronic charge transfer of CNL–ZnON'S, of its multiple layers and their adsorption configurations are shown in Table 4.6. The table shows that all the adsorption configurations of NH_3 on single– and multiple–layer CNL–ZnONS's have lower energy gaps compared to bare clusters of their corresponding CNL–ZnONS's. All the adsorption configurations of water on single– and multiple–layer CNL–ZnONS's have lower energy gaps compared to bare clusters of their corresponding CNL–ZnONS's except the adsorptions of which water molecule adsorbed at the edge within the outer and first inner layers. All chemical indices of bare single– and multiple–layer CNL–ZnONS's and their NH_3 and water adsorption configurations are not much difference except NH_3 dissociative adsorption on the single–layer CNL–ZnONS', H.NH$_2$/CNL–ZnONS' (1). Due to H.NH$_2$/CNL–ZnONS' (1) has very low energy gap (E_{gap}=1.318 eV) as compared with its bare CNL–ZnONS' (E_{gap}=3.290 eV), the single–layer CNL–ZnONS' may be applied as NH_3 sensor; its maximum electronic charge transfer is very high (ΔN_{max}= 6.175). The energy gap of dissociative adsorption configuration of water on the single–layer CNL–ZnONS', H.OH/CNL–ZnONS' (1) is somewhat low (E_{gap}=2.635 eV) and its adsorption energy is very high (ΔE_{ads}=–40.18 kcal/mol). Nevertheless, the single–layer CNL–ZnONS' can be used as water vapor absorber.

Table 4.5 Adsorption energies (ΔE_{ads} in kcal/mol) of NH_3 and H_2O on CNL–ZnONS'
and its multiple sheets, computed at the B3LYP/LanL2DZ level of theory.

Adsorption	ΔE_{ads}
NH_3 adsorbate	
Single layer cluster:	
NH_3 + CNL–ZnONS' → H.NH_2/CNL–ZnONS' (1)	−21.52
NH_3 + CNL–ZnONS' → NH_3/CNL–ZnONS' (2)	−28.25
Double layer cluster:	
NH_3 + (CNL–ZnONS')_2 → NH_3/(CNL–ZnONS')_2 (1)	−27.86
NH_3 + (CNL–ZnONS')_2 → NH_3/(CNL–ZnONS')_2 (2)	−24.54
Triple layer cluster:	
NH_3 + (CNL–ZnONS')_3 → NH_3/(CNL–ZnONS')_3 (1)	−27.25
NH_3 + (CNL–ZnONS')_3 → NH_3/(CNL–ZnONS')_3 (2)	−22.18
Quadruple *layer cluster:*	
NH_3 + (CNL–ZnONS')_4 → NH_3/(CNL–ZnONS')_4 (1)	−28.25
NH_3 + (CNL–ZnONS')_4 → NH_3/(CNL–ZnONS')_4 (2)	−21.59
H_2O adsorbate	
Single layer cluster:	
H_2O + CNL–ZnONS' → H.OH/CNL–ZnONS' (1)	−40.18
H_2O + CNL–ZnONS' → H_2O/CNL–ZnONS' (2)	−28.52
Double layer cluster:	
H_2O + (CNL–ZnONS')_2 → H_2O/(CNL–ZnONS')_2 (1)	−27.04
H_2O + (CNL–ZnONS')_2 → H_2O/(CNL–ZnONS')_2 (2)	−28.24
Triple layer cluster:	
H_2O + (CNL–ZnONS')_3 → H.OH/(CNL–ZnONS')_3 (1)	−30.24
H_2O + (CNL–ZnONS')_3 → H_2O/(CNL–ZnONS')_3 (2)	−29.11
H_2O + (CNL–ZnONS')_3 → H_2O/(CNL–ZnONS')_3 (3)	−25.32
Quadruple layer cluster:	
H_2O + (CNL–ZnONS')_4 → H_2O/(CNL–ZnONS')_4 (1)	−30.01
H_2O + (CNL–ZnONS')_4 → H_2O/(CNL–ZnONS')_4 (2)	−29.12
H_2O + (CNL–ZnONS')_4 → H_2O/(CNL–ZnONS')_4 (3)	−12.03
H_2O + (CNL–ZnONS')_4 → H_2O/(CNL–ZnONS')_4 (4)	−13.72

Table 4.6 HOMO–LUMO gaps (E_{gap}), chemical indices and electronic charge transfer of adsorption configuration of multiple layer CNL–ZnONS' species.

Species	E_{gap} [a]	η [a,b]	S [c]	μ [a,d]	χ [a,e]	ω [a,f]	ΔN_{max} [g]
Bare clusters:							
CNL–ZnONS'	3.290	1.645	0.304	−4.916	1.645	7.345	2.988
(CNL–ZnONS')$_2$	3.447	1.724	0.290	−4.800	1.724	6.683	2.785
(CNL–ZnONS')$_3$	3.210	1.605	0.312	−4.755	1.605	7.042	2.962
(CNL–ZnONS')$_4$	3.300	1.650	0.303	−4.755	1.650	6.851	2.882
NH$_3$ adsorption							
H.NH$_2$/CNL–ZnONS' (1)	1.318	0.659	0.759	−4.068	0.659	12.561	6.175
NH$_3$/CNL–ZnONS' (2)	3.044	1.522	0.329	−4.536	1.522	6.759	2.980
NH$_3$/(CNL–ZnONS')$_2$ (1)	3.298	1.649	0.303	−4.517	1.649	6.185	2.739
NH$_3$/(CNL–ZnONS')$_2$ (2)	3.145	1.573	0.318	−4.460	1.573	6.325	2.836
NH$_3$/(CNL–ZnONS')$_3$ (1)	3.115	1.557	0.321	−4.532	1.557	6.595	2.910
NH$_3$/(CNL–ZnONS')$_3$ (2)	3.031	1.516	0.330	−4.528	1.516	6.764	2.988
NH$_3$/(CNL–ZnONS')$_4$ (1)	3.206	1.603	0.312	−4.558	1.603	6.480	2.843
NH$_3$/(CNL–ZnONS')$_4$ (2)	3.204	1.602	0.312	−4.595	1.602	6.588	2.868
H$_2$O adsorption							
H.OH/CNL–ZnONS'(1)	2.635	1.318	0.379	−4.756	1.318	8.583	3.609
H$_2$O/CNL–ZnONS' (2)	3.293	1.646	0.304	−4.768	1.646	6.905	2.896
H$_2$O/(CNL–ZnONS')$_2$ (1)	3.444	1.722	0.290	−4.690	1.722	6.386	2.724
H$_2$O/(CNL–ZnONS')$_2$ (2)	3.488	1.744	0.287	−4.705	1.744	6.347	2.698
H$_2$O/(CNL–ZnONS')$_3$ (1)	3.116	1.558	0.321	−4.766	1.558	7.288	3.059
H$_2$O/(CNL–ZnONS')$_3$ (2)	3.218	1.609	0.311	−4.671	1.609	6.780	2.903
H$_2$O/(CNL–ZnONS')$_3$ (3)	3.068	1.534	0.326	−4.594	1.534	6.879	2.995
H$_2$O/(CNL–ZnONS')$_4$ (1)	3.228	1.614	0.310	−4.771	1.614	7.053	2.956
H$_2$O/(CNL–ZnONS')$_4$ (2)	3.309	1.654	0.302	−4.685	1.654	6.633	2.832
H$_2$O/(CNL–ZnONS')$_4$ (3)	2.996	1.498	0.334	−4.518	1.498	6.813	3.016
H$_2$O/(CNL–ZnONS')$_4$ (4)	3.269	1.634	0.306	−4.669	1.634	6.670	2.857

[a] In eV.

[b] Chemical hardness, $\eta = E_{gap}/2$.

[c] Chemical softness, $S = 1/E_{gap}$, in eV^{-1}.

[d] Electronic chemical potential, $\mu = (E_{HOMO} + E_{LUMO})/2$.

[e] The Mulliken electronegativity, $\chi = -(E_{HOMO} + E_{LUMO})/2$.

[f] The electrophilicity, $\omega = \mu^2/2\eta$.

[g] The maximum electronic charge transfer, $\Delta N_{max} = -\dfrac{\mu}{\eta}$.

CHAPTER V

Conclusions

The structures of non− (ZnOGLNS's) and hydrogen−terminated ZnO graphene−like nanosheets (ZnOGLNSs) and their multi−layers $(PRL–ZnONS)_n$, $(CNL–ZnONS)_n$, (n = 2 to 4) and $(CCL–ZnONS)_n$, (n = 2) were obtained using B3LYP/LanL2DZ calculations. Three pairs of structure comparisons between non− and hydrogen−terminated nanosheets as PRL–ZnONS' vs PRL–ZnONS, CNL−ZnONS' vs CNL−ZnONS and CCL−ZnONS' vs CCL−ZnONS are in the same symmetrical groups but their hexagonal rings are differently distorted from the perfect ring. All interlayer distances for non−terminated forms of double−, triple− and quadruple−layer ZnOGNSs are much shorter than that of non−terminated (ZnOGNS's) corresponding forms. For interlayer distances of each non–terminated double−layer, triple−layer, quadruple−layer for either PRL−ZnOGNS or CNL−ZnOGNS or CCL−ZnOGNS are quite equal and equivalent. The stepwise binding energies of PRL–ZnONS's, CNL–ZnONS's and CCL–ZnONS's systems are the same sequences. The first, second and third stepwise binding energies for ZnONS's and ZnONSs systems are in the same orders: PRL–ZnONS' > CNL–ZnONS' > CCL–ZnONS and PRL–ZnONS > CNL–ZnONS > CCL–ZnONS', respectively.

The adsorption configurations of NH_3 adsorption on the single−, double−, triple− and quadruple−layer CNL–ZnONS's are composed of two configurations for each. All adsorption configurations are non–dissociative adsorption except one of the NH_3 on the single–layer CNL–ZnONS' which is dissociative. The adsorption configurations of water adsorption on the single–, double–, triple– and quadruple–layer CNL–ZnONS's are composed of two, two, three and four configurations, respectively. Adsorption energies of CNL–ZnOGLNS' and its multi–layers species are within –28.25 to –21.52 kcal/mol for NH_3 and –40.18 to –12.03 kcal/mol for H_2O, respectively. All chemical indices of bare single– and multiple–layer CNL–ZnONS's and their NH_3 and water adsorption configurations are not much difference except NH_3 dissociative adsorption on the single–layer CNL–ZnONS', H.NH_2/CNL–ZnONS'

(1). Due to H.NH$_2$/CNL–ZnONS' (1) has very low energy gap (E_{gap} = 1.318 eV) as compared with its bare CNL–ZnONS' (E_{gap} = 3.290 eV), the single–layer CNL–ZnONS' may be applied as NH$_3$ sensor. The energy gap of dissociative adsorption configuration of water on the single–layer CNL–ZnONS', H.OH/CNL–ZnONS' (1) is somewhat low (E_{gap} = 2.635 eV) and its adsorption energy is very high (ΔE_{ads} = –40.18 kcal/mol). Therefore, the single–layer CNL–ZnONS' can be used as water vapor absorber.

REFERENCES

[1]   Malloci, G., Chiodo, L., Rubio, A., and Mattoni, A. Structural and optoelectronic properties of unsaturated ZnO and ZnS nanoclusters. J. Phys. Chem. C 116 (2012): 8741–8746.

[2]   Azpiroz, J.M., Mosconi, E., and Angelis, F.D. Modeling ZnS and ZnO nanostructures: structural, electronic, and optical properties. J. Phys. Chem. C 115 (2011): 25219–25226.

[3]   Yong, Y., Song, B., and He, P. Growth pattern and electronic properties of cluster–assembled material based on $Zn_{12}O_{12}$: a densitry–functional study. J. Phys. Chem. C 115 (2011): 6455–6461.

[4]   Chen, H., Ding, J., Yuang, N., Wang, X., Chen, C., and Weng, D. First–principle study of interaction H_2 and H_2O molecules with $(ZnO)_n$ (n=3–6) ring clusters . Proc. Nat. Sci. 20 (2010): 30–37.

[5]   Qiang, T., Yafei, L., Yonhsheng, C., and Zhongfang, C. Tuning electronic and nagnetic properties of wurtzite ZnO nanosheets by surface hydrogenation. ACS Appl. Mater. Interfaces 2 (2010): 2442–2447.

[6]   Morkoç, H., and Özgür, Ü. Zinc oxide: fundamentals, materials and device technology. Wiley–VCH Verlag, GmbH & Co, 2009.

[7]   Cheng, X., Li, Feng., and Zhao, Y. A DFT investigation on ZnO clusters and nanostructure. J. Mol. Struct. Theochem 894 (2009): 121–127.

[8]   Wang, F., and *et al*. Photoluminescence characteristics of ZnO clusters confined in the micropored of zeolite L. J. Phys. Chem. C 111 (2009): 121–127.

[9]   Hao, M., Xia, Y., Tan, Z., Liu, X., and Mei, L. Design and energetic characterization of ZnO clusters from first–principles and calculations. Phys. Lett. A. 372 (2007): 39–43.

[10]   Jain, A., Kumar, V., and Kawazoe, Y. Ring structures of small ZnO clusters. J. Am. Chem. Soc. 102 (2006): 6752–6761.

[11]   Lima, R.C., and *et al*. Toward and understanding of intermediate– and short–rang defects in ZnO crystals. A combined experimental theoretical study. J. Phys. Chem. A 112 (2008): 8970–8978.

[12] Zhou, Z., Li, Y., Liu, L., Chen, Y., Zhang, S. B. and Chen, Z. Size– and surface dependent stability, electronic properties, and potential as chemical sensors: computational studies on one-dimensional ZnO nanostructures. J. Phys. Chem. C 112 (2008): 13926–13931.

[13] Xiao, Q., Huang, S., Zhang, J., Xiao, C., and Tan, X. Sonochemical synthesis of ZnO nanosheet. J. Alloys. Compd. 459 (2008): 18–22.

[14] Martin, L. B. L., Taft, C. A., Lie, S. K., and Longo, E. Lateral interaction of CO and H_2 molecules on ZnO surface: an AM1 surfaces. J. Mol. Struct. Theochem 528 (2000): 161–170.

[15] Lu, X., Xu, X., Wang, N., and Zhang, Q. Heterolytic adsorption of H_2 on ZnO (1010) surface: An ab initio SPC cluster model study. J. Phys. Chem. B 103 (1999): 2689–2695.

[16] Liu, Y., Zeng, J., Zhang, J., Xu, F., and Sun, L. Improved hydrogen storage in the modified metal–organic frameworks by hydrogen spillover effect. Int. J. Hydrogen Energy 32 (2007): 4005–4015.

[17] Torres, F.J., Vitillo, J.G., Civalleri, B., Ricchiardi, G., and Zecchina, A. Interaction of H_2 with alkali–metal–exchanged zeolited: a quantum mechanical study. J. Phys. Chem. C 111 (2007): 2505–2518.

[18] Han, S.S., Deng, W–Q., and Goddard III, W.A. Improved designs of metal–organic frameworks for hydrogen storage. Angew. Chem. Int. Ed. 46 (2007): 6289–6292.

[19] Kuc, A., Zhechkov, L., Patchkovskii, S., Seifert, G., and Heine, T. Hydrogen sieving and storage in fullerence intercalated graphite. Nano Lett. 7 (2007): 1–5.

[20] Reddy, A.L.M., Ramaprabhu, S. Hydrogen adsorption properties of single–walled carbon nanotube–nanocrystal platinum composites. Int. J. Hydrogen Energy 33 (2008): 1028–1034.

[21] Lyakutti, K., Kawazoe, Y., Rajarajeswari, M., and Surya, V.J. Aluminum hydride coated single–wall carbon nanotube as a hydrogen storage medium. Int. J. Hydrogen Energy 34 (2009): 370–375.

[22] Liu, W., Zhao, Y.H., Jiang, Q., and Lavernia, E.J. Enhanced hydrogen storage on Li–dispersed carbon nanotubes. <u>J. Phys. Chem. C</u> 113 (2009): 2028–2051.

[23] Li, J., Cheng, S., Zhao, Q., Long, P., and Dong, J. Synthesisi and hydrogen–storage behavior of metal–organic framwork MOF–5 <u>Int. J. Hydrogen Energy</u> 34 (2009): 1377–1382.

[24] Luzan, S.M., Jung, H., Chun, H., and Talyzin, A.V. Hydrogen storage in Co and Zn–based metal–organic frameworks at ambient temperature. <u>Int. J. Hydrogen Energy</u> 34 (2009): 9754–0759.

[25] Ares, J.R., and *et al*. Hydrogen absorption/desorption mechanism in potassium alanate ($KAlH_4$) and enhancement by $TiCl_3$ doping. <u>J. Phys. Chem. C</u> 113 (2009): 6845–6851.

[26] Novaković, N., and *et al*. Ab initio calculations of MgH2, MgH2:Ti and MgH2:Co compounds. <u>Int. J. Hydrogen Energy</u> 35 (2010): 598–608.

[27] Calleja, G., and *et al*. Hydrogen adsorption over zeolite–like MOF materials modified by ion exchange. <u>Int. J. Hydrogen Energy</u> 35 (2010): 9916–9923.

[28] Zou, X., and et al. Hydrogen storage in Ca–decorated, B–substituted metal organic framework. <u>Int. J. Hydrogen Energy</u> 35 (2010): 198–203.

[29] Maark, T.A., and Pal, S. A model study effect of M = Li^+, Na^+, Be^{2+}, and Al^{3+} ion decoration adsorption of metal–organic framework–5. <u>Int. J. Hydrogen Energy</u> 35 (2010): 12846–12903.

[30] Yang, S.J., Cho, J.H., Nahm, K.S., and Park, C.R. Enhanced hydrogen storage capacity of Pt–loaded CNT@MOF–5 hybrid composites. <u>Int. J. Hydrogen Energy</u> 35 (2010): 13062–13069.

[31] Li, F., Zhao, J., Johansson, B., and Sun, L. Improving hydrogen storage properties of covalent organic frameworks by substitutional doping. <u>Int. J. Hydrogen Energy</u> 35 (2010): 266–271.

[32] Park, H.L., Yi, S.C., and Chung, Y.C. Hydrogen adsorption on Li metal in boron–substituted graphene: An *ab initio* approach. <u>Int. J. Hydrogen Energy</u> 35 (2010): 3583–3587.

[33] Lopez–Corral, I., German, E., Volpe, M.A., Brizuela, G.P., and Juan, A. Tight–binding study of hydrogen adsorption on palladium decorated graphene and carbon nanotubes. J. Hydrogen Energy 35 (2010): 2377–2384.

[34] Dimit, M., Maark, T.A., and Pal, S. *Ab initio* and periodic DFT investigation of hydrogen storage on light metal–decorated MOF–5. Int. J. Hydrogen Energy 36 (2011): 10816–10827.

[35] Prakash, M., Elango, M., and Subramanian, V. Adsorption of hydrogen molecules on the alkali metal ion decorated boric clusters: A density functional theory investigation. Int. J. Hydrogen Energy 36 (2011): 3922–3931.

[36] Böyükata, M., and Güvenc, Z.B. DFT study of Al doped cage $B_{12}H_n$ clusters. Int. J. Hydrogen Energy 36 (2011): 8392–8402.

[37] Signal, A., Rojas, M.I., Leiva, E.P.M. Interferents for hydrogen storage on a graphene sheet decorated with nickel: A DFT study. Int. J. Hydrogen Energy 36 (2011): 3537–3546.

[38] Gopalsamy, K., Prakash, M., Kumar, R.M., and Subramanian, V. Density functional studies on the hydrogen storage capacity of boranes and alanes based cages. Int. J. Hydrogen Energy 37 (2012): 9730–9741.

[39] López–Corral, I, and *et al.* DFT study of H2 adsorption on Pd–decorated single walled carbon nanotubes with C–vacancies. Int. J. Hydrogen Energy 37 (2012): 10156–10164.

[40] López–Corral, I, and *et al.* Hydrogen adsorption on palladium dimer decorated graphene: Abonding study. Int. J. Hydrogen Energy 37 (2012): 6653–6665.

[41] Zhang, Z.W., Zheng, W.T., and Jiang, Q. Hydrogen adsorption on Ce/BNNT systems: A DFT study. Int. J. Hydrogen Energy 37 (2012): 5090–5099.

[42] Dixit, D.K., Gandhi, K., and Dixit, B.K. Theoretical calculation of hydrogen desorption energies of calcium hydride clusters. Int. J. Hydrogen Energy 37 (2012): 3767–3771.

[43]   Kaewruksa, B., and Ruangpornvisuti, V. Theoretical study on the adsorption behaviors of H_2O and NH_3 on hydrogen–terminated ZnO nanoclusters and ZnO graphene–like nanosheets. J. Mol. Struct. 994 (2011): 276–282.

[44]   Kaewruksa, B., and Ruangpornvisuti, V. First principle investigation of oxygen adsorption on hydrogen–terminated ZnO graphene–like nanosheets. J. Mol. Struct. 18 (2012): 1447–1454.

[45]   Kaewruksa, B., and Ruangpornvisuti, V. Co–adsorptions of CO/N_2O, NO/NH_3, CO_2/N_2 and conversion of CO/N_2O to CO_2/N_2 on ZnO graphene–like sheet. J. Mol. Struct. 1012 (2012): 50–55.

[46]   Nakazawa, M., and Somorjai, G.A. Coadsorption of water and selected aromatic molecules to model the adhesion of epoxy resins on hydrated surfaces of zinc oxide and iron oxide. Appl. Surf. Sci. 84 (1995): 309

[47]   Martins, J.B.L., and *et al*. H_2O and H_2 interaction with ZnO surfaces: A MNDO, AM1, and PM3 theoretical study with large cluster model. Int. J. Quantum Chem. 57 (1996): 861.

[48]   Nagao, M., Kumashiro, R., Matsuda, T., and Kuroda, Y. Calorimetric study of water–two–dimensionally condensed on the homogeneous surface of a solid. Thermochim. Acta 253 (1995): 221.

[49]   Martin, J.B.L., and *et al*. The interaction of H_2, CO, CO_2, H_2O and NH_3 on ZnO surface: an oniom study. Chem. Phys. Lett. 400 (2004): 481.

[50]   Calzolari, A., and Catellani, A. Water adsorption on non–polar ZnO (1010) surface: a microscopic understanding. J. Phys. Chem. C 113 (2009): 2896.

[51]   Levine, N. Quantum chemistry. 6th edition. Pearson prentice hall, 2010.

[52]   Cramer, C.J. Essentials of computational chemistry: theories and models 2nd edition. Singapore: John Wiley and Sons, 2004.

[53]   Engel, T., and Reid, P. Physical chemistry. Pearson benjamin chummings, 2009.

[54]   Lewars, E. Computational chemistry. Canada: Trent University, 2003.

[55]   Frisch, M.J., et al. Gaussian 03, revision D.02, gaussian Inc. wallingford. CT, 2006.

[56] Kong, S., Shenderovich, G., and Vener, M.V. Density functional study of the proton transfer effect on vibrations of strong (short) intermolecular O–H···N/O⁻···H–N⁺ hydrogen bonds in aprotic solvents. <u>J. Phys. Chem. A</u> 114 (2010): 2393–2399.

[57] Kohn, W., Becke, A.D. and Parr, R.G. Density functional theory of eletronic structure. <u>J. Phys Chem.</u> 100 (1996): 12974–12980.

[58] Parr, R.G., Donnelly, R.A., Levy, M. and Palke, W.E. Electronegativity: The density functional view point. <u>J. Chem. Phys</u> 68 (1978): 3801.

[59] Parr, F.A., Srivastana, H.K., Beg, Y. and Singh, P.P. DFT Based Electrophilicity Index and QSAR study of Phenols as Anti Leukaemia Agent. <u>Am. J. Immunology 2</u> 1 (2006): 23–28.

[60] Parr, R.G. and Pearson, R.G. Absolute hardness: comparrion parameter to absolute electronegavity. <u>J. Am. Chem. Soc.</u> 105 (1983): 7512.

[61] Yang, W. and Parr, R.G. Hardness, softness, and fukui function in the electronic theory of metal and catalysis. <u>Proc. Natl. Acad. Sci</u> 82 (1985): 6723.

[62] Ghosh, S.K. and Berkowitz, M. A classical fluid–like approch to the density functional formalism of many-electron systems. <u>J. Chem. Phys.</u> 83 (1985): 2976.

[63] Parr, R.G. and Yang, W. Density functional approach to the frontier-electron theory of chemical reactivity. <u>Proc. Natl. Acad. Sci</u> 82 (1985): 6723.

[64] Yang, W. and Mortier, W.J. The use of global and local molecular parameters for the analysis of the gas-phase basicity of amines. <u>J. Am. Chem. Soc.</u> 108 (1986): 5708.

[65] Sabin, J.R., Trickey, S.P., Apee, J. and Oddershede, J. Molecular shape, capacitance, and chemical hardness. <u>Int. J. Quantum Chem.</u> 77 (2000): 358.

[66] Parr, R.G. and Yang, W. Density functional approach to the frontier–electron theory of chemical reactivity. <u>Proc. Natl. Acad. Sci</u> 82 (1985): 6723.

[67] Parr, R.G., Szentpaly, Lv. and Liu, S. Electrophilicity Index. <u>J. Am. Chem. Soc.</u> 121 (1999): 1922.

[68] Chattaraj, P.K., Pérez, P., Zevallos, J. and Toro–Labbé, A. Ab initio SCF and DFT studied on solvent effects of intramolecular rearrangement reaction. J. Phys. Chem. A 105 (2001): 4272.

[69] Pérez, P., Toro–Labbé, A. and Contreras, R. Solvent effects on electrophilicity. J. Am. Chem. Soc. 123 (2001): 5527.

[70] Chattaraj, P.K., Pérez, P., Zevallos, J. and Toro–Labbé, A. Solvent effects on trans–$N_2H_2 \rightarrow$ cis–N_2H_2 and $F_2S_2 \rightarrow$ FSSF reaction in gas and solution phase. J. Mol Struct. Theochem 580 (2002): 171.

[71] Pérez, P., Toro–Labbé, A., Aizman, A. and Contreras, R. Comparison between experimental and theoretical scale of electrophilicity in benzhydryl cations. J. Org. Chem. 67 (2002): 4747.

[72] Jaque, P. and Toro–Labbé, A. Characterization of copper cluster through the use of density functional theory reactivity descriptors. J. Chem Phys. 117 (2002): 3208.

[73] Koopmans, T. Ordering of wave functions and eigenergies to the individual electrons of an atom. Physica 1. 123 (2001): 104.

APPENDIX
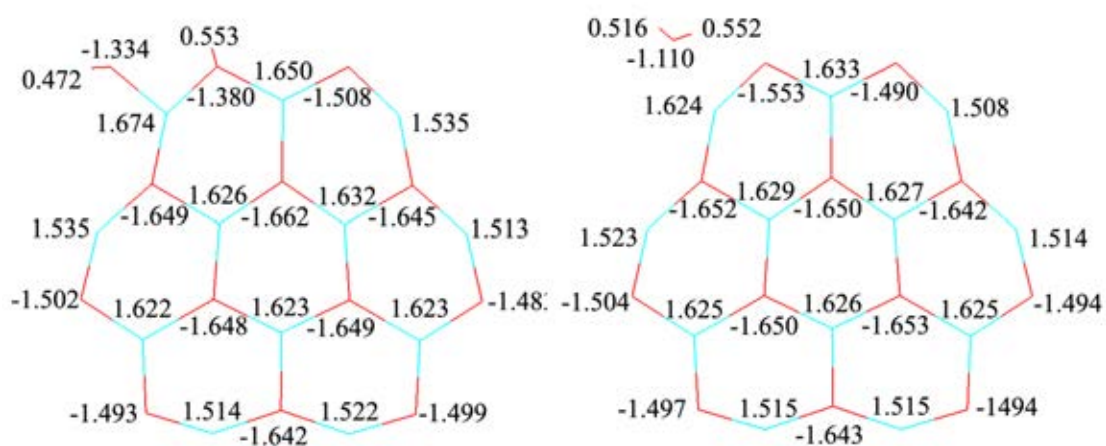
Figure A-1. NBO charges of water adsorption on CNL–ZnONS' (left) H.OH/ CNL–ZnONS' and (right) H_2O/ CNL–ZnONS'.
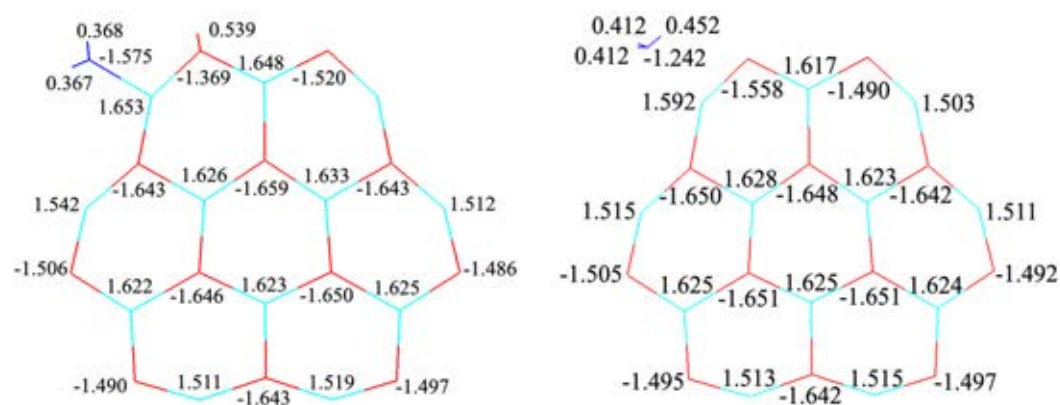
Figure A-2 NBO charges ammonia adsorption on CNL–ZnONS' (left) H.OH/ CNL–ZnONS' and (right) H_2O/ CNL–ZnONS'.
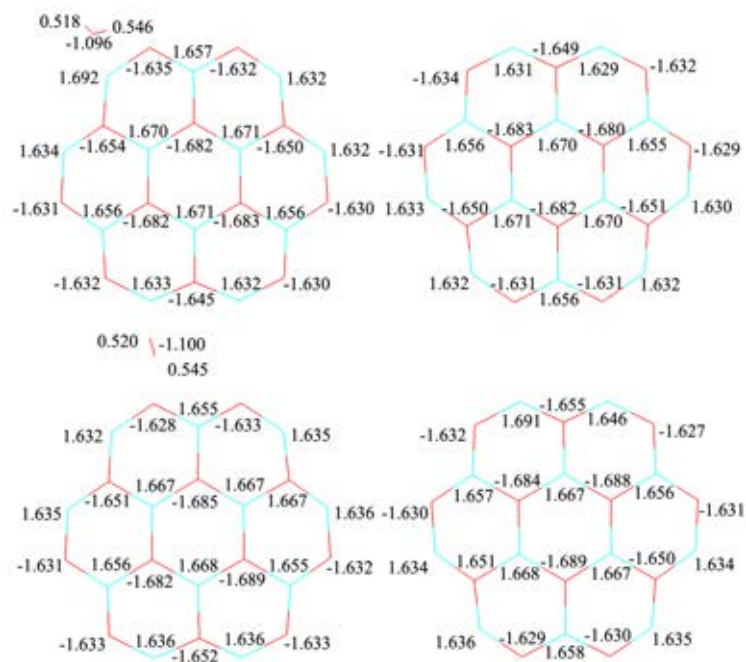
Figure A-3 NBO charges water adsorption on (CNL–ZnONS')$_2$ (left) H.OH/ CNL–ZnONS' and (right) H$_2$O/ CNL–ZnONS'.
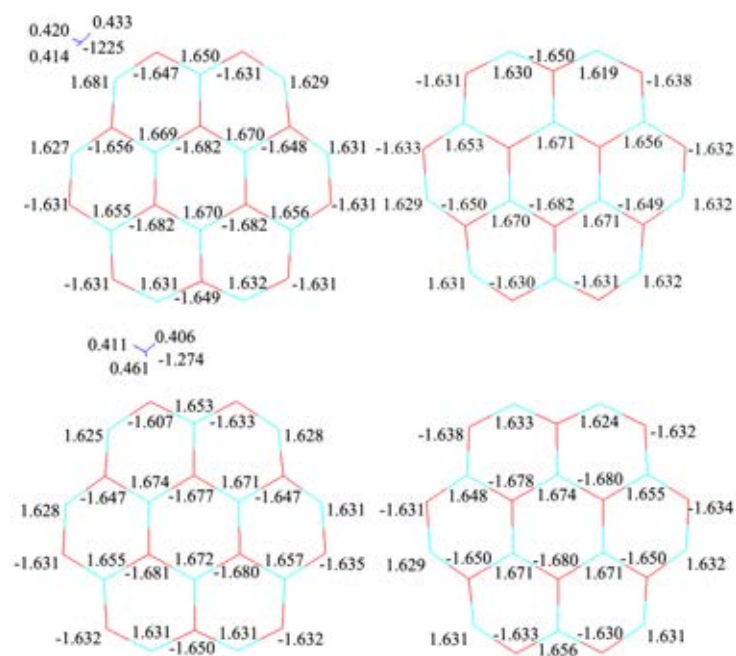
Figure A-4 NBO charges ammonia adsorption on (CNL–ZnONS')$_2$ (left) H.OH/ CNL–ZnONS' and (right) H$_2$O/ CNL–ZnONS'.
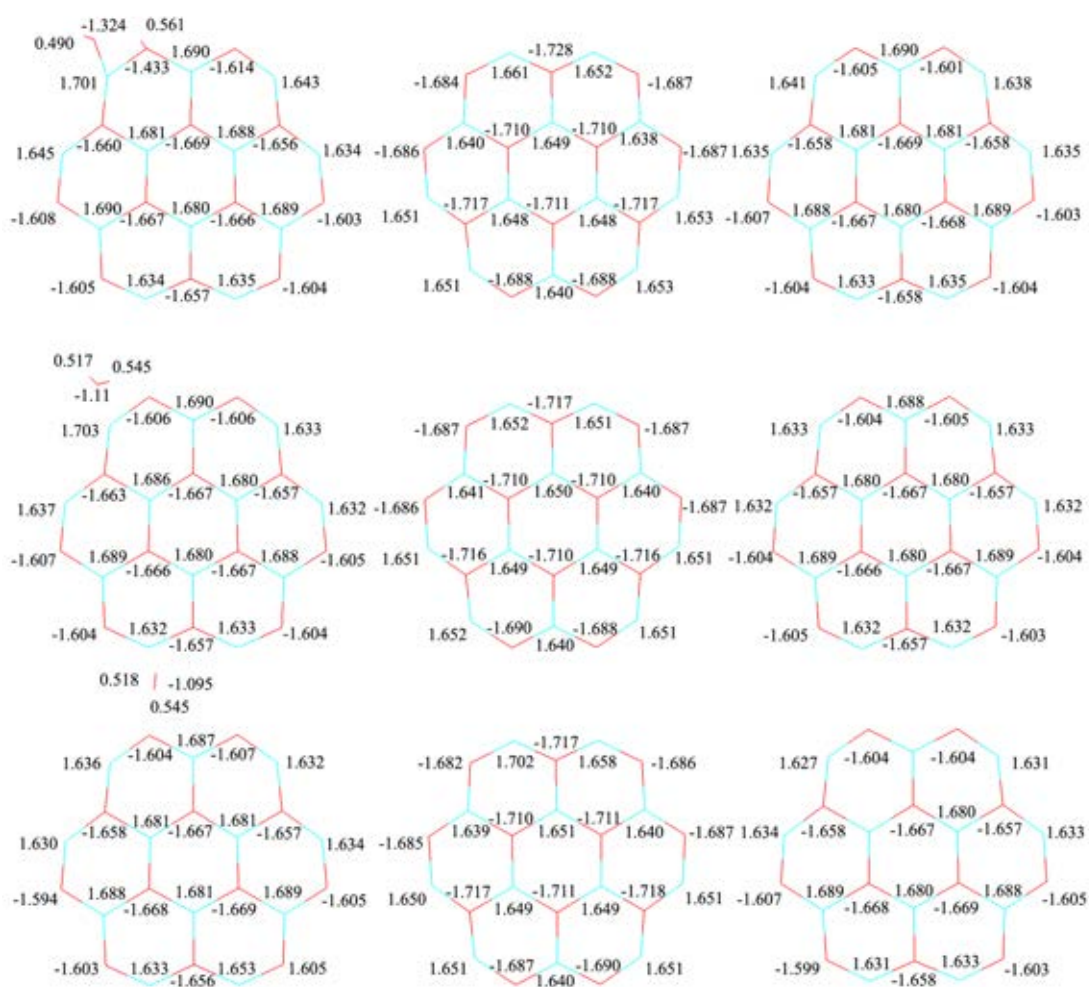
Figure A-5 NBO charges water adsorption on (CNL–ZnONS')$_3$ (top) H.OH/ CNL–ZnONS', (middle) H$_2$O/ CNL–ZnONS' (1) and (bottom) H$_2$O/ CNL–ZnONS' (2).

Figure A-6 NBO charges ammonia adsorption on (CNL–ZnONS')₃ (top) NH₃/ CNL–ZnONS' (1), (middle) NH₃/ CNL–ZnONS' (2) and (bottom) NH₃/ CNL–ZnONS' (3).
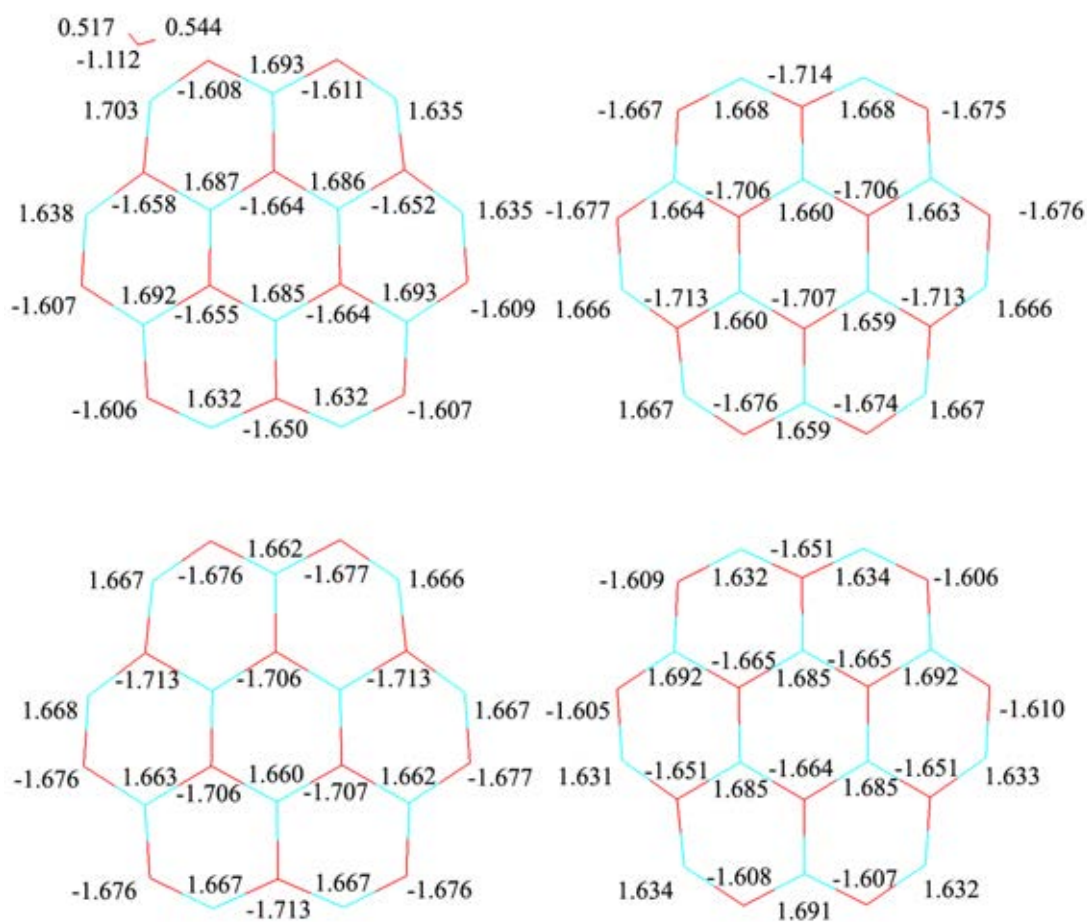
Figure A-7 NBO charges water adsorption on (CNL–ZnONS')$_4$(1) top line, (left): first layer, (right): second layer, bottom line, (left): third layer, (right): fourth layer.
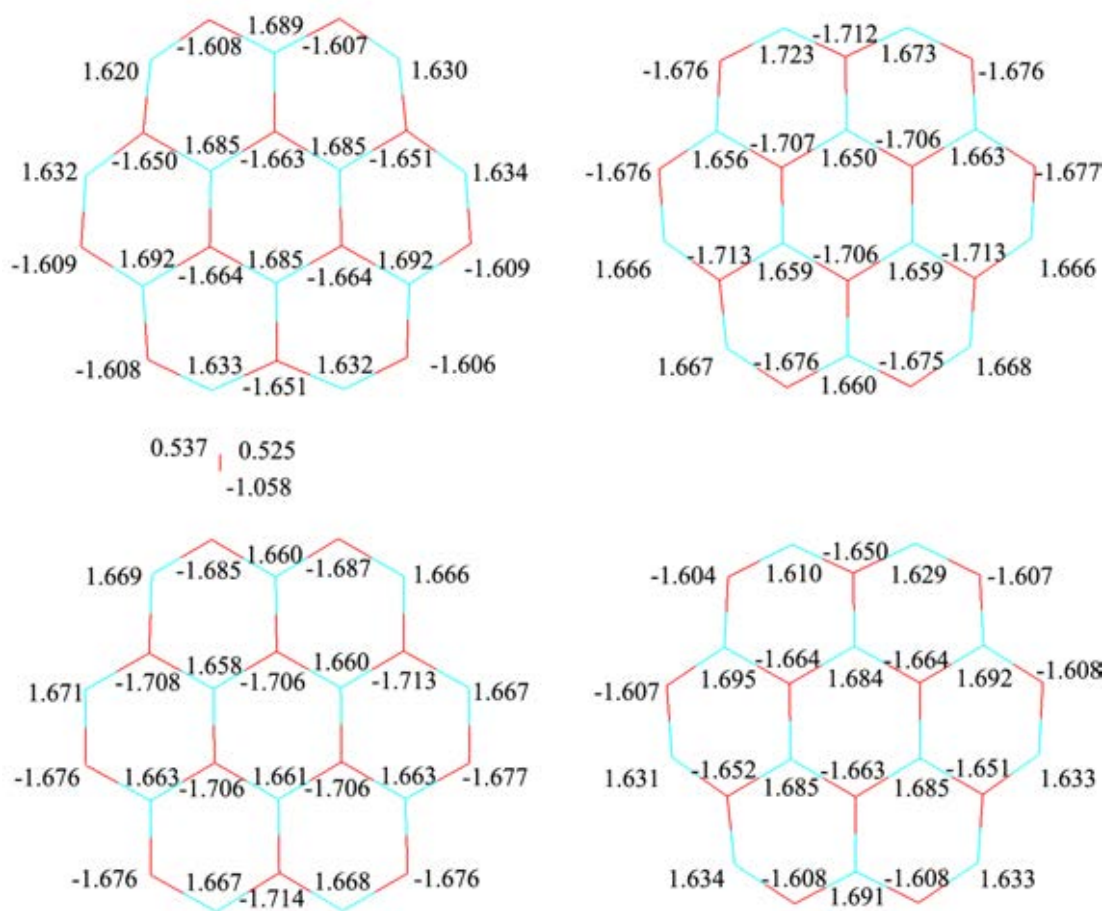
Figure A-8 NBO charges water adsorption on (CNL–ZnONS')$_4$(2) top line, (left): first layer, (right): second layer, bottom line, (left): third layer, (right): fourth layer.

0.515

0.543 -1.106

1.708
1.635 -1.598 -1.628 1.630
1.685 1.684
1.634 -1.652 -1.663 -1.651 1.634
1.692 1.685 1.692
-1.608 -1.664 -1.664 -1.608
-1.607 1.634 1.633 -1.607
-1.652

-1.709
1.713 1.677
-1.674 -1.672
-1.706 -1.706
-1.676 1.662 1.659 1.662 -1.676
-1.713 -1.706 -1.713
1.666 1.659 1.659 1.667
-1.676 -1.675
1.667 1.660 1.668

1.645
1.670 -1.676 -1.660 1.671
1.658 1.659
1.668 -1.713 -1.706 -1.713 1.667
1.663 1.660 1.663
-1.667 -1.706 -1.706 -1.667
1.676 1.668 1.668 1.677
-1.714

-1.654
1.632 1.629
-1.609 -1.609
-1.663 -1.663
-1.606 1.691 1.684 1.692 -1.606
-1.652 -1.663 -1.652
1.632 1.684 1.685 1.633
1.634 -1.608 -1.609 1.633
1.691

Figure A-9 NBO charges water adsorption on (CNL–ZnONS')$_4$(3) top line, (left): first layer, (right): second layer, bottom line, (left): third layer, (right): fourth layer.
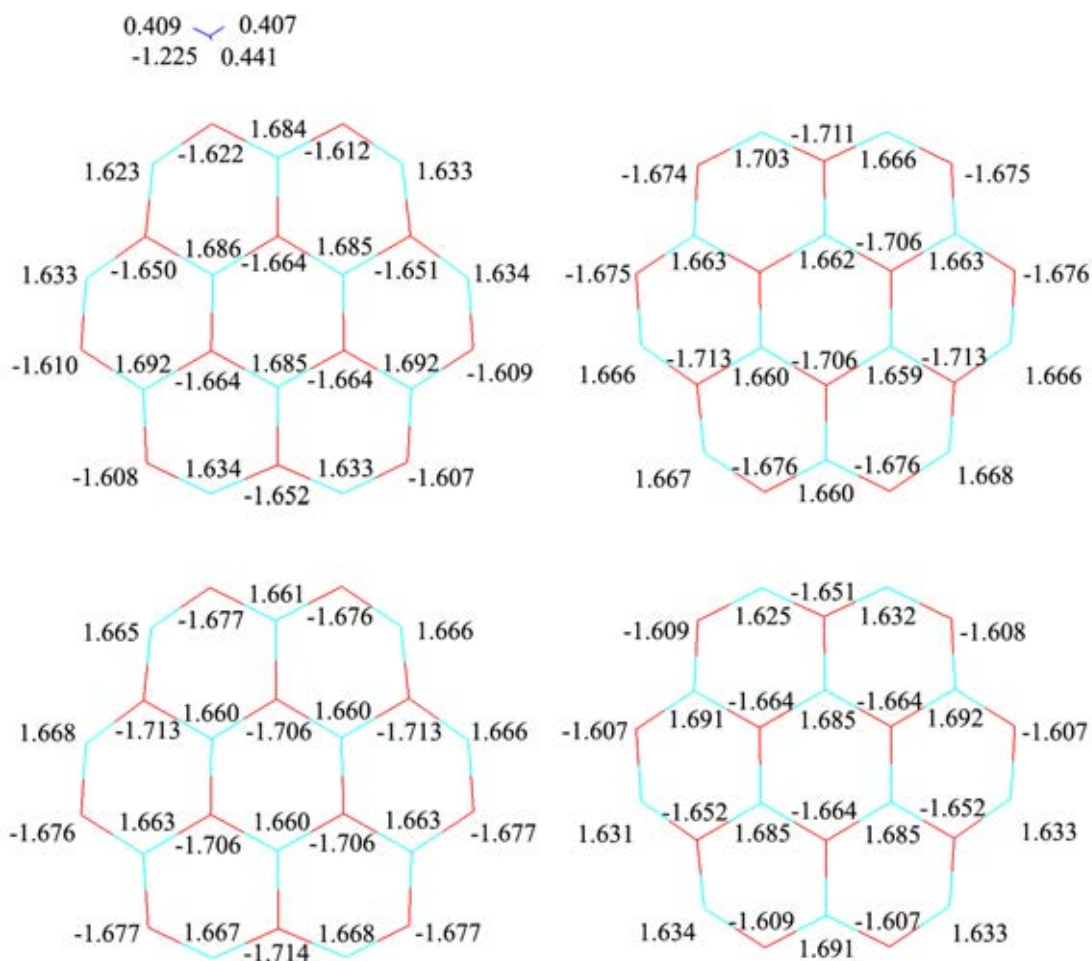
Figure A-10 NBO charges ammonia adsorption on (CNL–ZnONS')₄ (1) top line, (left): first layer, (right): second layer, bottom line, (left): third layer, (right): fourth layer.

Table A-1 Selected geometrical parameters of non– and hydrogen–terminated structures for PRL–ZnONSs[a].

Data/Species	PRL–ZnONS'	PRL–ZnONS	Difference
Bond length (Å)			
O1–Zn1	1.85	1.99	0.14
O2–Zn1	1.86	1.96	0.10
O2–Zn2	2.05	1.92	–0.13
O2–Zn3	1.90	1.93	0.03
O3–Zn2	1.88	1.98	0.10
O3–Zn4	2.11	1.89	–0.22
O4–Zn3	1.79	2.05	0.26
O4–Zn4	1.93	1.96	0.03
O5–Zn4	1.88	1.96	0.08
O5–Zn5	1.83	1.99	0.16
Bond angle(°)			
O1–Zn1–O2	136.98	108.13	–28.85
Zn1–O1–Zn1'	100.78	136.98	36.20
Zn1–O2–Zn2	119.34	118.66	–0.68
Zn1–O2–Zn3	141.57	110.13	–31.44
O2–Zn2–O3	126.69	115.29	–11.40
O2–Zn3–O4	145.53	108.22	–37.31
Zn2–O3–Zn4	121.68	119.50	–2.18
Zn3–O4–Zn4	114.89	120.05	5.16
O3–Zn4–O5	120.70	117.33	–3.37
O4–ZN4–O5	127.19	120.98	–6.21
Zn4–O5–Zn5	108.98	129.97	20.99

[a] PRL–ZnONS' and PRL–ZnONS denote non– and hydrogen–terminated PRL–ZnONSs.

Table A-2 Selected geometrical parameters of non– and hydrogen–terminated structures for CNL–ZnONSs[a].

Data/Species	CNL–ZnONS'	CNL–ZnONS	Difference
Bond length (Å)			
O1–Zn1	1.91	1.93	0.02
O1–Zn2	1.80	2.03	0.23
O2–Zn1	2.10	1.89	–0.21
O2–Zn3	1.95	1.94	–0.01
O3–Zn2	1.86	1.94	0.08
O3–Zn3	2.02	1.92	–0.10
O3–Zn4	1.86	1.94	0.08
O4–Zn3	1.95	1.93	–0.02
O4–Zn5	2.10	1.89	–0.21
O4–Zn6	1.95	1.93	–0.02
O5–Zn4	1.80	2.03	0.23
O5–Zn5	1.91	1.93	0.02
O6–Zn6	2.02	1.92	–0.10
O6–Zn7	1.86	1.94	0.08
O7–Zn5	1.91	1.93	0.02
O7–Zn7	1.80	2.03	0.23
Bond angle(°)			
O1–Zn1–O1'	125.66	123.18	–2.48
O1–Zn1–O2	117.17	118.42	1.25
O1–Zn2–O3	144.58	109.19	–35.39
Zn1–O1–Zn2	109.46	127.31	17.85
Zn1–O2–Zn3	124.12	118.35	–5.77
Zn2–O3–Zn3	108.79	125.04	16.25
Zn2–O3–Zn4	142.43	109.85	–32.58
O2–Zn3–O4	128.25	116.71	–11.54
O3–Zn3–O4	115.87	121.59	5.72
O3–Zn4–O5	144.59	109.21	–35.38
Zn3–O4–Zn5	124.12	118.37	–5.75

[a] CNL–ZnONS' and CNL–ZnONS denote non– and hydrogen–terminated CNL–ZnONSs.

Table A-3 Selected geometrical parameters of non– and hydrogen–terminated structures for CCL–ZnONSs[a].

Data/Species	CCL–ZnONS'	CCL–ZnONS	Difference
Bond length (Å)			
O1–Zn1	1.93	1.97	0.04
O2–Zn1	1.93	1.91	–0.12
O2–Zn2	1.95	2.07	0.12
O3–Zn1	2.16	1.89	0.27
O3–Zn3	2.00	1.93	–0.07
O3–Zn4	1.98	1.96	–0.02
O4–Zn2	1.91	1.93	0.02
O4–Zn4	2.10	1.91	–0.19
O4–Zn5	1.92	1.93	0.01
O5–Zn3	2.00	1.91	–0.09
O5–Zn6	2.00	1.92	–0.08
O6–Zn4	2.00	1.93	–0.07
O6–Zn6	2.00	1.92	–0.08
O6–Zn7	2.00	1.93	–0.07
O7–Zn5	1.92	1.98	0.06
O7–Zn7	2.10	1.91	–0.19
O7–Zn8	1.91	1.93	0.02
O8–Zn6	1.99	1.92	–0.07
O8–Zn9	2.00	1.91	–0.09
O9–Zn7	1.98	1.96	–0.02
O9–Zn9	2.00	1.93	–0.07
O9–Zn10	2.16	1.89	–0.27
O10–Zn8	1.95	2.07	0.12
O10–Zn10	1.93	1.91	–0.02
O11–Zn10	1.93	1.97	0.04
Bond angle(^{o})			
Zn1–O1-Zn1'	127.90	121.61	–6.29
O1–Zn1–O2	126.19	121.49	–4.70
O1–Zn1–O3	113.19	117.54	4.35
Zn1–O2–Zn2	119.60	126.09	6.49
Zn1–O3–Zn3	120.13	121.91	1.78
Zn1–O3–Zn4	120.23	116.74	–3.49
O2–Zn2–O4	128.79	107.58	–21.21
Zn2-O4-Zn4	112.49	127.85	15.36
Zn2-O4-Zn5	128.27	110.83	–17.44
O3–Zn3–O5	119.91	120.26	0.35
O3–Zn4–O4	119.55	120.73	1.18
O3–Zn4–O6	121.16	116.98	–4.18
Zn3–O3–Zn4	119.40	121.35	1.95
Zn4–O4–Zn5	112.53	121.31	8.78
Zn3–O5–Zn6	120.22	119.22	–1.00
Zn4–O6–Zn6	119.42	121.38	–1.96
Zn4–O6–Zn7	121.04	117.20	–3.84
O4–Zn5–O7	128.48	115.60	–12.88

[a] CCL–ZnONS' and CCL–ZnONS denote non– and   hydrogen–terminated CCL–ZnONSs.

Table A-4 Selected geometrical parameters of bond distances (Å) between non– and hydrogen–terminated PRL–ZnONSs [a].

Bond distances/Species	Double	Triple		Quadruple		
	1/2	1/2	2/3	1/2	2/3	3/4
PRL–ZnONS':						
O1–Zn5	2.07	2.05	2.05	2.07	1.99	2.08
O2–Zn4	2.87	2.29	2.29	2.35	2.05	2.23
O3–Zn2	2.25	2.26	2.26	2.18	2.35	2.15
O4–Zn3	2.03	2.04	2.04	2.04	2.06	2.05
O5–Zn1	2.04	2.05	2.05	2.03	2.07	2.01
PRL–ZnONS:						
O1–Zn5	2.11	2.23	2.41	2.38	2.22	4.13
O2–Zn4	2.31	2.15	2.16	2.15	2.35	2.18
O3–Zn2	2.09	2.17	2.15	2.21	2.12	2.28
O4–Zn3	2.27	2.88	2.17	2.12	2.90	2.17
O5–Zn1	2.32	2.20	3.03	3.11	2.14	2.82

[a] PRL–ZnONS' and PRL–ZnONS denote non– and hydrogen–terminated PRL–ZnONSs.

Table A-5 Selected geometrical parameters of bond distances (Å) between non– and hydrogen–terminated CNL–ZnONSs[a].

Bond distances/Species	Double	Triple		Quadruple		
	1/2 [b]	1/2 [b]	2/3 [c]	1/2 [b]	2/3 [c]	3/4 [d]
Non–terminated CNL–ZnONS:						
O1-Zn7	2.02	2.05	2.04	2.05	2.05	2.05
O2-Zn6	2.23	2.27	2.27	2.22	2.25	2.20
O3-Zn5	3.05	2.30	2.31	2.30	2.07	2.21
O4-Zn3	2.25	2.27	2.27	2.23	2.25	2.20
O5-Zn4	2.02	2.05	2.05	2.05	2.05	2.06
O6-Zn1	3.05	2.30	2.31	2.31	2.08	2.21
O7-Zn2	2.03	2.05	2.04	2.05	2.05	2.05
Hydrogen–terminated CNL–ZnONS:						
O1-Zn7	2.30	2.25	2.67	2.16	2.87	2.20
O2-Zn6	2.38	2.22	2.20	2.24	2.14	2.25
O3-Zn5	2.09	2.15	2.15	2.18	2.32	2.21
O4-Zn3	2.39	2.22	2.20	2.24	2.14	2.24
O5-Zn4	2.28	2.27	2.63	2.16	2.84	2.21
O6-Zn1	2.09	2.15	2.15	2.19	2.32	2.21
O7-Zn2	2.28	2.25	2.67	2.14	2.91	2.19

[a] CNL–ZnONS' and CNL–ZnONS denote non– and hydrogen–terminated CNL–ZnONSs.

[b] Bond distances between the first and second layers.

[c] Bond distances between the second and third layers.

[d] Bond distances between the third and fourth layers.

Table A-6 Selected geometrical parameters of bond distances (Å) between non– and hydrogen–terminated CCL–ZnONSs[a].

Bond distances/Species	Double	Triple		Quadruple		
	1/2 [b]	1/2 [b]	2/3 [c]	1/2 [b]	2/3 [c]	3/4 [d]
Non–terminated CCL–ZnONS:						
O1-Zn14	1.98	2.08	2.08	2.01	2.22	2.02
O2-Zn15	2.03	2.07	2.07	2.06	2.07	2.05
O3-Zn12	2.30	2.04	2.05	2.28	2.25	2.26
O4-Zn13	2.97	2.39	2.39	2.28	2.09	2.35
O5-Zn11	2.28	2.27	2.27	2.29	2.39	2.28
O6-Zn9	2.22	2.31	2.30	2.45	2.22	2.35
O7-Zn10	2.98	2.40	2.40	2.27	2.08	2.35
O8-Zn6	2.28	2.27	2.27	2.29	2.39	2.28
O9-Zn7	2.30	2.05	2.05	2.27	2.22	2.26
O10-Zn8	2.03	2.07	2.07	2.05	2.10	2.06
O11-Zn5	1.98	2.08	2.07	2.05	2.25	2.03
O12-Zn4	2.30	2.05	2.05	2.05	2.10	2.06
O13-Zn3	2.22	2.40	2.40	2.27	2.22	2.27
Hydrogen–terminated CCL–ZnONS:						
O1-Zn14	3.81	–	–	–	–	–
O2-Zn15	2.24	–	–	–	–	–
O3-Zn12	2.27	–	–	–	–	–
O4-Zn13	2.09	–	–	–	–	–
O5-Zn11	2.30	–	–	–	–	–
O6-Zn9	2.37	–	–	–	–	–
O7-Zn10	2.09	–	–	–	–	–
O8-Zn6	2.30	–	–	–	–	–
O9-Zn7	2.27	–	–	–	–	–
O10-Zn8	2.24	–	–	–	–	–
O11-Zn5	3.82	–	–	–	–	–
O12-Zn4	2.27	–	–	–	–	–
O13-Zn3	2.36	–	–	–	–	–

[a] CCL–ZnONS' and CCL–ZnONS denote non– and   hydrogen–terminated CCL–ZnONSs.

[b] Bond distances between the first and second layers.

[c] Bond distances between the second and third layers.

[d] Bond distances between the third and fourth layers.

VITAE

Name:	Miss CHALITA MEKMUKDA
Date of Birth:	October 12th, 1986
Place of Birth:	Saraburi, Thailand
Address:	1415/272 Life @ Phahol–Ari Phaholyothin Road, Bangkok 10400, Thailand
Telephone:	082–3677712
E-mail address:	mkchalita@gmail.com
Educations:	
2010-2012	M.Sc. (Physical Chemistry), Chulalongkorn University, Thailand
2005-2008	B.Sc. (Chemistry), Chulalongkorn University, Thailand
2001-2004	Triamudomsuksa high school, Bangkok, Thailand
1998-2000	Suranari Withaya secondary school, Nakonratchasima, Thailand
1992-1997	Nakonratchasima primary school, Nakonratchasima, Thailand
Presentation:	
2013	Adsorption of NH_3 on ZnO nanosheets for gas sensor (Poster Session): The 3rd Hatyai symposium, May 10 2013 at Hatyai University, Songkla, Thailand.